

## Sulphur simulations for East Asia using the MATCH model with meteorological data from ECMWF

Magnuz Engardt

Cover: Deduced total sulphur deposition in East Asia, using an anthropogenic sulphur emission inventory valid for 1993 and meteorological data for January and May 1993. Units, g sulphur m<sup>-2</sup> year<sup>-1</sup>.

**Sulphur simulations for East Asia  
using the MATCH model with  
meteorological data from ECMWF**

**Magnuz Engardt**



# Report Summary / Rapportsammanfattning

|   |                             |                             |
|---|-----------------------------|-----------------------------|
| Issuing Agency/Utgivare   | Report number/Publikation   |                             |
| Swedish Meteorological and Hydrological Institute<br>S-601 76 NORRKÖPING<br>Sweden  | RMK No. 88                  | Report date/Utgivningsdatum |
|   |                             | March 2000                  |
| Author (s)/Författare<br>Magnuz Engardt (magnuz.engardt@smhi.se)  |                             |                             |
| Title (and Subtitle)/Titel<br>Sulphur simulations for East Asia using the MATCH model with meteorological data from ECMWF   |                             |                             |
| Abstract/Sammandrag<br><p>As part of a model intercomparison exercise, with participants from a number of Asian, European and American institutes, sulphur transport and conversion calculations were conducted over an East Asian domain for 2 different months in 1993. All participants used the same emission inventory and simulated concentration and deposition at a number of prescribed geographic locations. The participants were asked to run their respective model both with standard parameters, and with a set of given parameters, in order to examine the different behaviour of the models. The study included comparison with measured data and model-to-model intercomparisons, notably source-receptor relationships.</p> <p>We hereby describe the MATCH model, used in the study, and report some typical results. We find that although the standard and the prescribed set of model parameters differed significantly in terms of sulphur conversion and wet scavenging rate, the resulting change in atmospheric concentrations and surface depositions only change marginally. We show that it is often more critical to choose a representative gridbox value than selecting a parameter from the suite available.</p> <p>The modelled, near-surface, atmospheric concentration of sulphur in eastern China is typically 5-10 <math>\mu\text{g S m}^{-3}</math>, with large areas exceeding 20 <math>\mu\text{g S m}^{-3}</math>. In southern Japan the values range from 2-5 <math>\mu\text{g S m}^{-3}</math>. Atmospheric <math>\text{SO}_2</math> dominates over sulphate near the emission regions while sulphate concentrations are higher over e.g. the western Pacific. The sulphur deposition exceeds several g sulphur <math>\text{m}^{-2} \text{year}^{-1}</math> in large areas of China. Southern Japan receives 0.5-1 g S <math>\text{m}^{-2} \text{year}^{-1}</math>. In January, the total wet deposition roughly equals the dry deposition, in May – when it rains more in the domain – total wet deposition is ca. 50% larger than total dry deposition.</p> |                             |                             |
| Key words/sök-, nyckelord<br>MATCH, sulphur, transport modelling, acid deposition, East Asia  |                             |                             |
| Supplementary notes/Tillägg   | Number of pages/Antal sidor | Language/Språk              |
|   | 33                          | English                     |
| ISSN and title/ISSN och titel<br>0347-2116 SMHI Reports Meteorology Climatology   |                             |                             |
| Report available from/Rapporten kan köpas från:<br>SMHI<br>S-601 76 NORRKÖPING<br>Sweden  |                             |                             |



# Sulphur simulations for East Asia using the MATCH model with meteorological data from ECMWF

Magnuz Engardt  
Swedish Meteorological and Hydrological Institute  
S-601 76 Norrköping  
SWEDEN

## Abstract

As part of a model intercomparison exercise, with participants from a number of Asian, European and American institutes, sulphur transport and conversion calculations were conducted over an East Asian domain for 2 different months in 1993. All participants used the same emission inventory and simulated concentration and deposition at a number of prescribed geographic locations. The participants were asked to run their respective model both with standard parameters, and with a set of given parameters, in order to examine the different behaviour of the models. The study included comparison with measured data and model-to-model intercomparisons, notably source-receptor relationships.

We hereby describe the MATCH model, used in the study, and report some typical results. We find that although the standard and the prescribed set of model parameters differed significantly in terms of sulphur conversion and wet scavenging rate, the resulting change in atmospheric concentrations and surface depositions only change marginally. We show that it is often more critical to choose a representative gridbox value than selecting a parameter from the suite available.

The modelled, near-surface, atmospheric concentration of sulphur in eastern China is typically 5-10  $\mu\text{g S m}^{-3}$ , with large areas exceeding 20  $\mu\text{g S m}^{-3}$ . In southern Japan the values range from 2-5  $\mu\text{g S m}^{-3}$ . Atmospheric  $\text{SO}_2$  dominates over sulphate near the emission regions while sulphate concentrations are higher over e.g. the western Pacific. The sulphur deposition exceeds several  $\text{g sulphur m}^{-2} \text{year}^{-1}$  in large areas of China. Southern Japan receives 0.5-1  $\text{g S m}^{-2} \text{year}^{-1}$ . In January, the total wet deposition roughly equals the dry deposition, in May – when it rains more in the domain – total wet deposition is ca. 50% larger than total dry deposition.

## 1. Introduction

Asia is the home of over 3 billion people, and its population is steadily increasing. On top of that, many Asian countries host booming economies with rapid expansion of public and private production and consumption. The energy demands for the region is mainly satisfied through the usage of fossil fuel. Therefore, anthropogenic emissions of many pollutants, such as e.g. nitrogen oxides ( $\text{NO}_x$ ), and sulphur dioxide ( $\text{SO}_2$ ), are increasing and are likely to increase in the future (Rodhe et al., 1992; Rodhe, 1999; et al., 1999; Aardenne et al., 1999). The usage of coal, which is readily available in many countries, and has a high sulphur to energy ratio, is expected to lead to particularly high sulphur emissions (Lefohn et al., 1999), in case no active measures are taken to reduce the emissions. Anthropogenic emissions of  $\text{NO}_x$  and  $\text{SO}_2$  will eventually lead to increased depositions of acids, such as nitric acid ( $\text{HNO}_3$ ) and sulphuric acid ( $\text{H}_2\text{SO}_4$ ), and many areas in Asia do have a high sensitivity for

ecosystem damage due to acidic deposition (Kuylenstierna et al., 1995). This is a situation similar to the European and North American scene, several decades ago, which eventually lead to environmental degradation through the acidification of soils and lakes. See the *Acid Reign '95* conference summary statement (Rodhe et al., 1995).

Acid deposition is a typical regional problem with long-range transport of precursor species from the emission regions to the subsequent deposition in areas, which may lie thousands of km away. The problem has been studied extensively in Europe and North America, and to some extent also in Asia. Current Asian studies include monitoring activities, aimed at determining the natural background, and the enhanced levels near the emission regions (e.g. Carmichael et al., 1995; Ayers et al., 1996; Granat et al., 1996; Fern and Rodhe, 1997), as well as model studies aimed at quantifying the dispersion and chemical conversion of natural or anthropogenic species (e.g. Hayami, and Ichikawa, 1995; Ichikawa and Fujita, 1995; Arndt et al., 1998; Phadnis et al., 1998; Xu and Carmichael, 1998; 1999). Traditionally sulphur has been studied most extensively since it is believed to contribute the most to enhanced acid deposition.

MATCH (Multiple-scale Atmospheric Transport and CHEMical modelling system) is a versatile, moderately sophisticated, tool for simulating transport, deposition and chemical conversion of atmospheric pollutants. It is a Eulerian model that runs "off-line"; i.e. the driving meteorological data are taken from an external source, typically the analysis, or the forecast, from a dynamical weather prediction model. MATCH is developed for maximal flexibility with regards to model domain and resolution, and it is possible to choose between different deposition and chemical conversion routines.

Earlier versions of MATCH have previously been used for applications in the tropics, see e.g. Robertson et al. (1995; 1996), and Hicks et al. (1998). The current report describes an effort to run MATCH over an East Asian domain. The study is performed in parallel with several other modelling groups with the ultimate goal of comparing the performance of different models operating in the region. In this larger study, all groups employ a linear transformation of SO<sub>2</sub> to sulphate. For the dry deposition, a standard, deposition velocity approach, is used. Wet deposition, finally, is parameterised from the surface precipitation and a bulk scavenging coefficient.

A detailed description of the implementation of the advection and the boundary layer parameterisation in MATCH can be found in Robertson et al. (1996; 1999). Examples of different regional-scale applications in different geographic areas are found in Langner et al. (1995; 1996; 1998a; 1998b), Engardt and Holmén (1996; 1999), Robertson and Langner (1998).

The current report will go through the adopted strategy for deposition and chemical conversion of SO<sub>2</sub> and sulphate. We describe both the standard formulation (denoted Task A), and the alternative, prescribed, formulation (Task B), that was used in the intercomparison exercise. In the final, result section, we present some general results and also address the differences between the two formulations.

Since our calculations were performed with meteorological data from a different driver compared to most other groups in the study, we also briefly discuss the driving meteorological data. The final conclusions from the model intercomparison will be presented in a jointly authored paper elsewhere.

## 2. Description of the sulphur model

### 2.1 Dry Deposition

The dry deposition,  $D^j$  ( $\text{kg m}^{-2}$ ), of species  $j$  ( $\text{SO}_2$  or sulphate) is dependent on the “dry deposition velocity”,  $v_d^j$  ( $\text{m s}^{-1}$ ), and the tracer mass mixing ratio in the lowest model layer (denoted 1),  $\mu_1^j$  ( $\text{kg tracer per kg air}$ ), and is solved using a semi-implicit formulation,

$$D^j = \frac{v_d^j \mu_1^j \rho_1 \Delta t_{vdiff}}{1 + \alpha \left( \frac{g \rho_1}{\Delta p_1} v_d^j \Delta t_{vdiff} \right)} \quad (1)$$

$\rho_1$  ( $\text{kg m}^{-3}$ ) is the air density in the lowest model layer and  $\Delta t_{vdiff}$  (s) the time-step used for vertical diffusion, which can be any even fraction of the advection time-step,  $\Delta t_{adv}$ . Further,  $g$  ( $9.8 \text{ m s}^{-2}$ ) is the acceleration of gravity,  $\Delta p_1$  (Pa) is the depth of the lowest model layer and  $\alpha$  is a parameter determining the degree of implicitness in the scheme. Here we set  $\alpha=0.692$ , in accordance to Robertson et al. (1996; 1999).

As illustrated in Fig. 1, the vertical profiles of  $\text{SO}_2$ , and sulphate – both with a significant surface sink – will vary considerably, even within the lowest model layer.

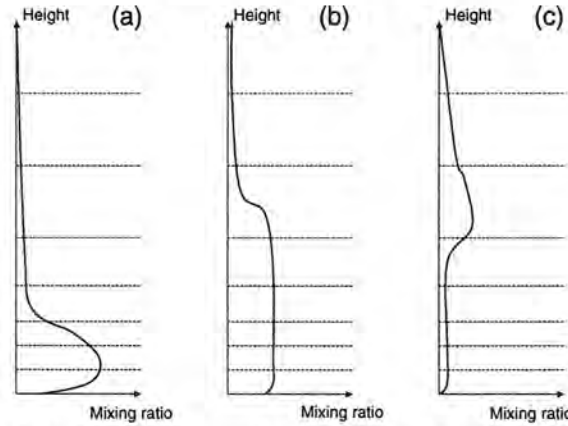


**Figure 1.** Schematic tracer profile under different stability conditions in the real world. (a) is a typical stable boundary layer; (b) is a well mixed boundary layer; (c) is a possible profile for a remote station downwind an emission area. Height and mixing ratio scales are arbitrary. Dashed lines represent model layers; in the current version of MATCH the lowest model layer is ~60 m thick.

The dry deposition velocity,  $v_d^j$ , is operating on the mean tracer mixing ratio in the lowest model layer,  $\mu_1^j$ . We therefore use Monin-Obukov similarity theory to convert the given deposition velocity,  $v_{d(1m)}^j$ , – which is assumed to be valid at 1 m height – to the middle of the lowest model layer, in order to retain a constant flux through the surface layer, see Fig. 2,

$$v_d^j = v_{d(1m)}^j F_{stab}^j \quad (2)$$

where,

$$F_{stab}^j = \frac{1}{1 + \frac{v_{d(1m)}^j}{ku_*} \left[ \ln\left(\frac{\Delta z_1}{2}\right) - \Psi_h\left(\frac{\Delta z_1}{2L}\right) + \Psi_h\left(\frac{1.0}{L}\right) \right]} \quad (3)$$

$k$  is von Karman's constant (0.4),  $u_*$  ( $\text{m s}^{-1}$ ) and  $L$  (m) are the friction velocity and the Monin-Obukov's length, respectively, both calculated in MATCH (see Robertson et al., 1996; 1999).  $\Delta z_1$  (m) is the thickness of the lowest model layer, and  $\Psi_h$  the "stability function for heat" (see e.g. Louis, 1979),

$$\Psi_h(\xi) = \begin{cases} 2 \ln\left(\frac{1+X}{2}\right), & \xi < 0 \\ -6.35\xi, & \xi \geq 0 \end{cases} \quad (4a)$$

and,

$$X = (1-9\xi)^{0.5}. \quad (4b)$$

Table 1 presents examples of the modification of  $v_{d(1m)}^j$  for different stability conditions. As can be noticed, the dry deposition velocity is reduced by 10-20 %, or more, during stable conditions but only change marginally in the convective boundary layer.

**Table 1.** Examples of the "stability parameter",  $F_{stab}^j$ , calculated from Eqs. (3)-(4) during different stability conditions. The lowest model layer is assumed to have a thickness of 60 m.

| $L$ (m)        | $v_{d(1m)}^j$ ( $\text{cm s}^{-1}$ ) | $F_{stab}^j$                      |                                   |                                   |
|----------------|--------------------------------------|-----------------------------------|-----------------------------------|-----------------------------------|
|                |                                      | $u_* = 0.1$ ( $\text{m s}^{-1}$ ) | $u_* = 0.3$ ( $\text{m s}^{-1}$ ) | $u_* = 0.5$ ( $\text{m s}^{-1}$ ) |
| + 40           | 0.1                                  | 0.83                              | 0.94                              | 0.96                              |
| (stable)       | 0.3                                  | 0.62                              | 0.83                              | 0.89                              |
| $\pm 2000$     | 0.1                                  | 0.92                              | 0.97                              | 0.98                              |
| (near neutral) | 0.3                                  | 0.79                              | 0.92                              | 0.95                              |
| - 40           | 0.1                                  | 0.95                              | 0.98                              | 0.99                              |
| (convective)   | 0.3                                  | 0.86                              | 0.95                              | 0.97                              |

The prescribed 1 m values of the dry deposition velocities in this study are given in Table 2. Note that the dry deposition was modelled identically in Task A and Task B and that all land cells were assigned the same value (i.e. no further split up into different surface types).

**Table 2.** Prescribed (Carmichael et al., 2000) dry deposition velocities,  $v_{d(1m)}^j$  (in  $\text{cm s}^{-1}$ ), used in the current study.

|                         | Land                          | Open water |
|-------------------------|-------------------------------|------------|
| $v_{d(1m)}^{SO_2}$      | 0.25 (May)<br>0.125 (January) | 0.32       |
| $v_{d(1m)}^{SO_4^{2-}}$ | 0.2                           | 0.1        |

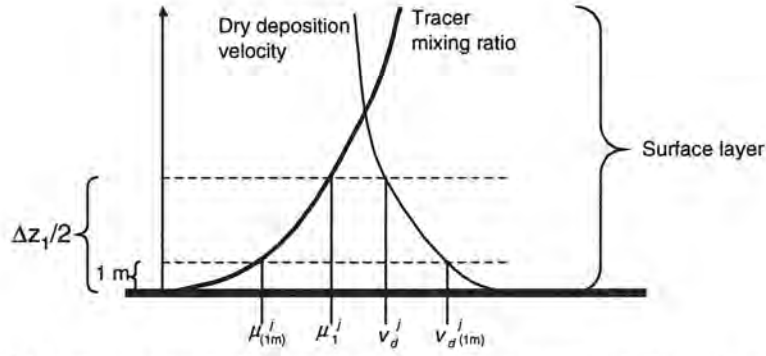


**Figure 2.** The relationship between tracer mixing ratio and the dry deposition velocity in the surface layer with constant flux  $F^j \sim v_d^j \times \mu_1^j = v_d^{j(1m)} \times \mu_{(1m)}^j$ . The tracer mixing ratio at the middle of the lowest model layer ( $z = \Delta z_1/2$ ) is taken as the mean layer mixing ratio.

## 2.2 Wet Deposition

The key parameters determining the wet deposition is the “*bulk scavenging coefficient*”,  $\Lambda^j$  ( $s^{-1}/(\text{mm h}^{-1})$ ), and the precipitation intensity at the surface,  $P_{surf}$  ( $\text{mm h}^{-1}$ ). Assuming that the precipitation scavenges tracer from the complete atmospheric column,  $\Lambda^j$  should ideally be determined from measurements of the column burden of a species and the surface deposition of that species.  $\Lambda^j$ , in the real world, is a function of cloud and precipitation type and vertical tracer profile, along with atmospheric ozone ( $\text{O}_3$ ) and hydrogen peroxide ( $\text{H}_2\text{O}_2$ )

concentrations. In this formulation,  $\Lambda^j$  represents both the *in-cloud* and the *sub-cloud*

scavenging of tracer  $j$ .  $\Lambda^{SO_2}$  also accounts for the *in-cloud* oxidation of  $\text{SO}_2$  to sulphate in precipitating clouds. Precipitation at the surface thus results in wet deposition of sulphate,  $W^{SO_4^{2-}}$  ( $\text{kg m}^{-2}$ ), and decreasing tracer mixing ratio (of both  $\text{SO}_2$  and sulphate) at all model layers,

$$W^{SO_4^{2-}} = \sum_{k=1}^{nlev} \frac{\Delta p_k}{g} \left( \frac{\Lambda^{SO_2} P_{surf} \mu_k^{SO_2} \Delta t_{vdiff}}{1 + \alpha(\Lambda^{SO_2} P_{surf} \Delta t_{vdiff})} + \frac{\Lambda^{SO_4^{2-}} P_{surf} \mu_k^{SO_4^{2-}} \Delta t_{vdiff}}{1 + \alpha(\Lambda^{SO_4^{2-}} P_{surf} \Delta t_{vdiff})} \right), \quad (5)$$

$$\Delta \mu_k^j = - \frac{\Lambda^j P_{surf} \mu_k^j \Delta t_{vdiff}}{1 + \alpha(\Lambda^j P_{surf} \Delta t_{vdiff})}. \quad (6)$$

$k$  indicates model level and  $j$  indicates each chemical species, note that  $\text{SO}_2$  and sulphate are always counted as sulphur.  $g$ ,  $\Delta p_k$ ,  $\Delta t_{vdiff}$ ,  $\mu_k^j$ , and  $\alpha$  has the same meaning and numerical values as in Eq. (1). Obviously, Eqs. (5) and (6) will decrease the tracer mixing ratio also above the precipitating cloud, which may cause too low simulated tracer concentrations in the upper troposphere, and too high surface depositions. However, the mixing ratio of  $\text{SO}_2$ , and sulphate is generally low above the mixed layer, and we therefore judge this inconsistency in the formulation as only a minor error.

Acknowledging the large uncertainty in choosing a representative value for  $\Lambda^j$ , and also the inherent temporal and spatial variability of this parameter, we have assigned constant values of  $\Lambda^{SO_2}$  and  $\Lambda^{SO_4^{2-}}$  for the standard (Task A) simulation according to Table 3 below. The chosen values are in the lower range of the numbers used for the normal mid-latitude MATCH applications.

For Task B, the wet deposition was modelled using a similar approach, but with different numerical values of  $\Lambda^j$ , and in the case of sulphate, also a power dependency of the surface precipitation (Carmichael et al., 2000). Table 3 details the formulation, and Fig. 3 displays the wet removal rate as a function of surface precipitation for the 2 formulations. As evident from Fig. 3, the standard (Task A) parameters are a factor of 2 more efficient to scavenge the tracers.

**Table 3.** Wet removal rate  $\Lambda^j \times (P_{surf})^n$  (in  $s^{-1}$ ), used in Task A and Task B simulations.

|                 | Task A                        | Task B                                |
|-----------------|-------------------------------|---------------------------------------|
| SO <sub>2</sub> | $40 \times 10^{-6} P_{surf}$  | $20 \times 10^{-6} P_{surf}$          |
| Sulphate        | $100 \times 10^{-6} P_{surf}$ | $50 \times 10^{-6} (P_{surf})^{0.83}$ |

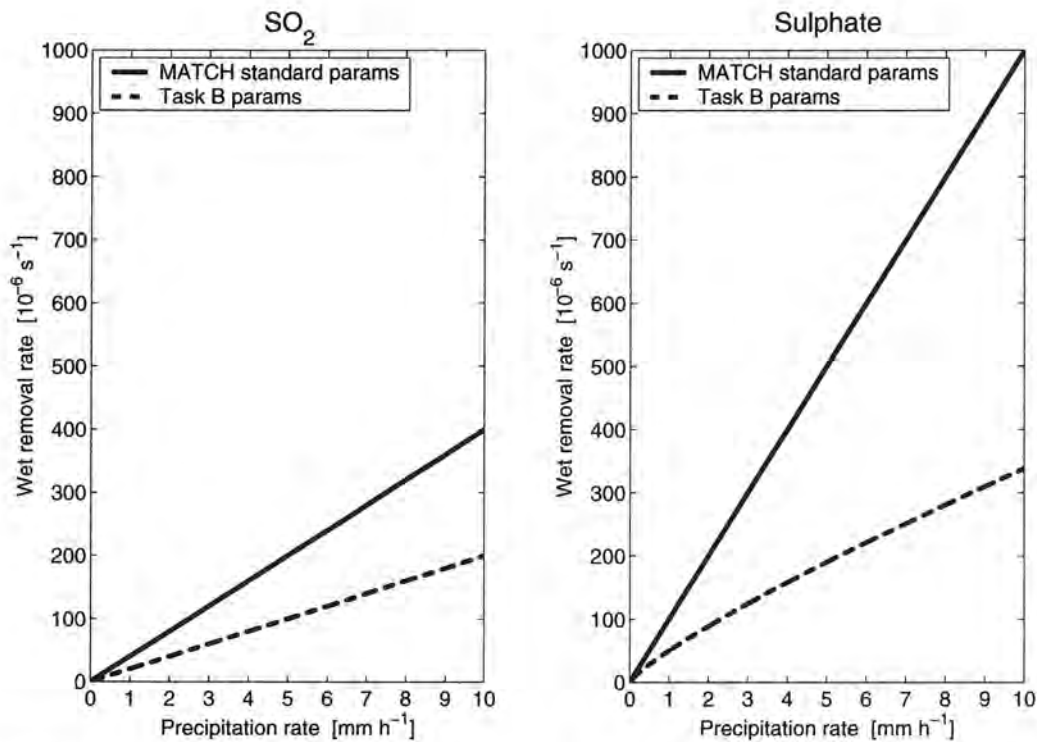


**Figure 3.** Wet removal rate of SO<sub>2</sub> and sulphate as a function of surface precipitation intensity. Solid line is standard (Task A) parameters, dashed line is Task B parameters.

### 2.3 Chemical conversion

There are several different chemical conversion schemes available in MATCH. The least sophisticated, which is chosen for the current simulations, is a linear transformation of SO<sub>2</sub> to sulphate,

$$\left(\mu_k^{SO_2}\right)^{t+\Delta t} = \left(\mu_k^{SO_2}\right)^t - \Delta\mu_k^{SO_2}, \quad (7)$$

$$\left(\mu_k^{sulphate}\right)^{t+\Delta t} = \left(\mu_k^{sulphate}\right)^t + \Delta\mu_k^{SO_2} \quad (8)$$

$(\mu_k^j)^{t+\Delta t}$  and  $(\mu_k^j)^t$  are the new and old mass mixing ratios of SO<sub>2</sub> and sulphate (counted as sulphur) at model level  $k$ .

$\Delta\mu_k^{SO_2}$  is the change in SO<sub>2</sub> (and sulphate) at every advection time-step  $\Delta t_{adv}$ ,

$$\Delta\mu_k^{SO_2} = k_{CH} \left(\mu_k^{SO_2}\right)^t \Delta t_{adv}. \quad (9)$$

In the standard (Task A) formulation, the conversion rate,  $k_{CH}$  (s<sup>-1</sup>), undergoes a diurnal cycle to account for the diurnal cycle in atmospheric OH concentration,

$$k_{CH} = \bar{k} - A \cos\left(\frac{2\pi H}{24}\right), \quad (10)$$

where  $H$  is local time (hours after midnight), and  $A$  (s<sup>-1</sup>), the amplitude of the diurnal cycle. Note that  $k_{CH}$  also accounts for the *in-cloud* oxidation of SO<sub>2</sub> to sulphate in *non-precipitating* clouds, which does not have pronounced diurnal cycle, thus the non-zero values of  $k_{CH}$  at night. The daily-mean value of  $k_{CH}$  is, of course, identical to  $\bar{k}$ , which varies linearly with latitude.  $\bar{k}$  is taken from Tarrasón and Iversen (1998),

$$\bar{k} = k_{EQ} + \frac{|\lambda|}{90} (k_{POLE} - k_{EQ}), \quad (11)$$

where  $\lambda$  is the latitude and

$$k_{POLE} = a + b \sin \gamma, \quad (12)$$

$$\gamma = \begin{cases} \frac{2\pi(\tau+91)}{365}, & \lambda < 0 \text{ (Southern Hemisphere)} \\ \frac{2\pi(\tau-91)}{365}, & \lambda \geq 0 \text{ (Northern Hemisphere)} \end{cases} \quad (13)$$

$\tau$  is the number of days since start of the year. This formulation yields a seasonally varying SO<sub>2</sub> to sulphate conversion rate, which reach a constant, maximum at the equator.

For Task B a similar formulation was utilised, with a constant, and high, conversion near the equator, and a seasonally varying component at the midlatitudes,

$$k_{CH} = k_0 f(\lambda) + k_1 [1 - f(\lambda)] \times g(\tau) \quad (14)$$

where,

$$f(\lambda) = \cos\left(\frac{\lambda \times 1.3\pi}{180}\right), \quad (15)$$

and

$$g(\tau) = \sin\left(\frac{(\tau - 80) \times 2\pi}{365}\right). \quad (16)$$

Note that (14)-(16) are only valid for  $\lambda < 55^\circ$  (Carmichael et al., 2000). Table 4 summarises the model parameters and Fig. 4 illustrates the seasonal and latitudinal variation of  $k_{CH}$  for Task A and B. Generally, Task B parameters yields a  $\text{SO}_2$  to sulphate conversion rate twice as fast as the standard (Task A) parameters.

**Table 4.** Parameter values for the chemical conversion models in the standard (Task A) and Task B simulations.

|          | Task A                                | Task B                                 |
|----------|---------------------------------------|--|
| A        | $0.4\bar{k}$                          |  |
| $k_{EQ}$ | $4.0 \times 10^{-6} \text{ s}^{-1}$ § |  |
| $a$      | $1.3 \times 10^{-6} \text{ s}^{-1}$ § |  |
| $b$      | $1.1 \times 10^{-6} \text{ s}^{-1}$ § |  |
| $k_0$    |                                       | $10.0 \times 10^{-6} \text{ s}^{-1}$ & |
| $k_1$    |                                       | $4.0 \times 10^{-6} \text{ s}^{-1}$ &  |

§ Tarrasón and Iversen (1998)

& Carmichael et al. (2000)

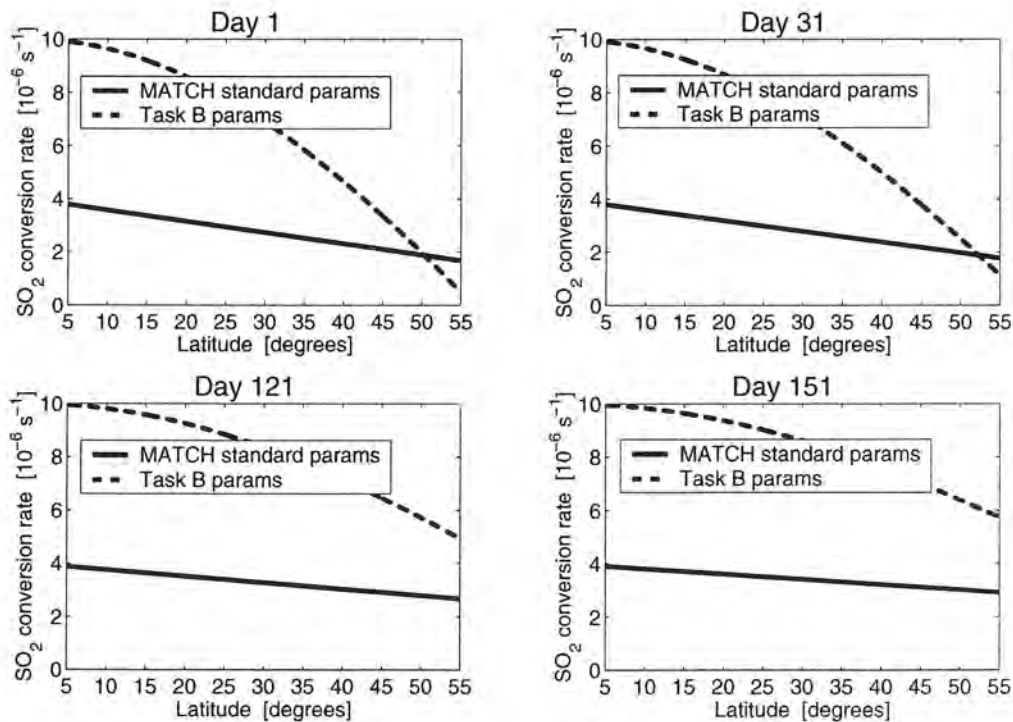


**Figure 4.** Daily-mean  $\text{SO}_2$  to sulphate conversion rate as a function of latitude. Solid line is standard (Task A) parameters, dashed line is Task B parameters. The 4 panels illustrates the conversion rate at day 1, 31, 121, 151 (beginning and end of January and May, respectively).

## 4. Set-up

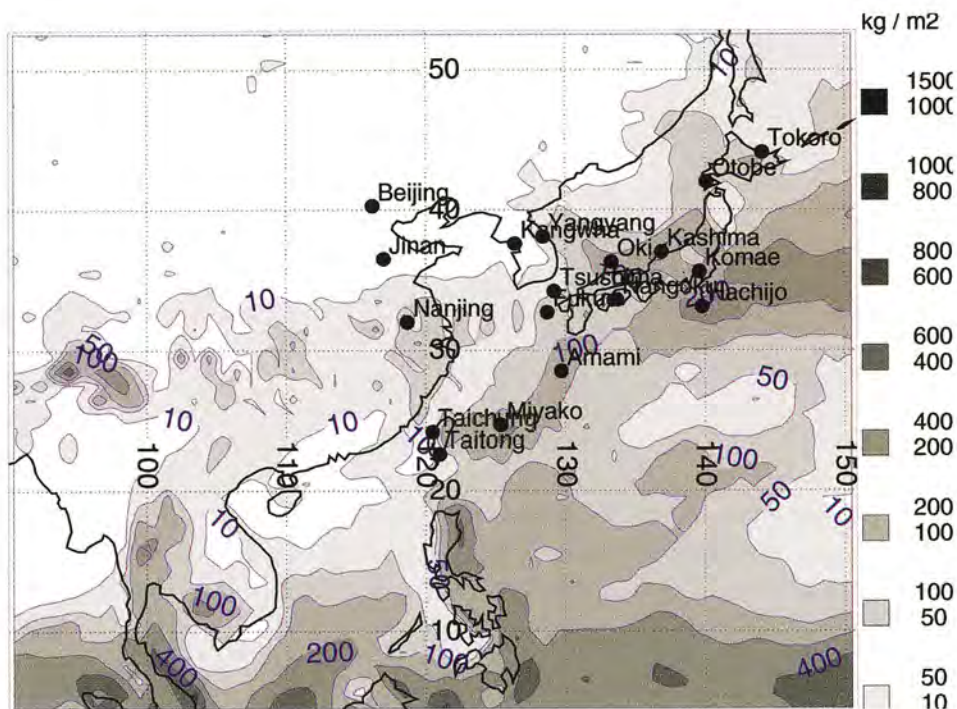
### 4.1 Meteorology

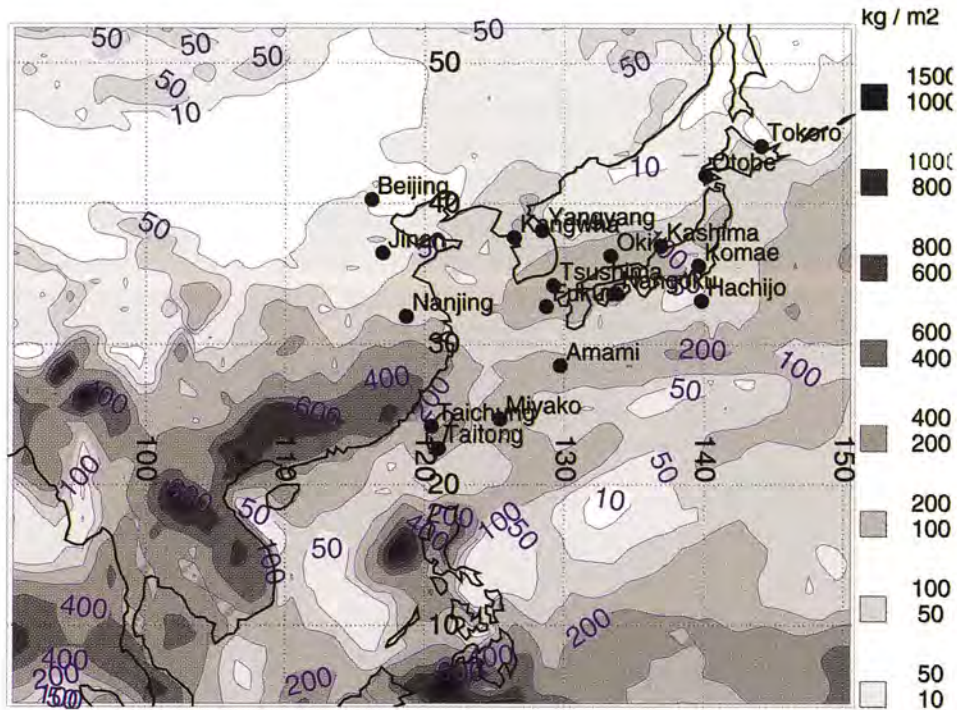
The model was run for 2 different months (January and May 1993) with meteorological data from ECMWF (European Centre for Medium-Range Weather Forecasts). We used the 6 hour “First Guess”, valid at 00, 06, 12, and 18Z. The data was interpolated from the T213 representation to a regular  $1^\circ \times 1^\circ$  latitude-longitude grid at ECMWF, and to 1 hour resolution internally in MATCH (Robertson et al., 1996; 1999).

**Table 5.** Parameters used in the current sulphur simulations  $N_{lon}$ ,  $N_{lat}$ , and  $N_{lev}$  are the number of gridpoints in the x, y, and z direction, respectively.

| Parameter          | Value  |
|--------------------|--------|
| $N_{lon}$          | 61     |
| $N_{lat}$          | 49     |
| $N_{lev}$          | 31     |
| West limit         | 90° E  |
| East limit         | 151° E |
| South limit        | 4° N   |
| North limit        | 53° N  |
| $\Delta t_{adv}$   | 600 s  |
| $\Delta t_{vdiff}$ | 600 s  |

The total precipitation, in the MATCH domain (see Table 5), as computed by ECMWF’s 6 hour “First guess” for January and May 1993, is given in Fig. 5. The total amount is larger in May than in January. This is especially true for most of South East Asia – including the high emission areas in southern China – where it rains substantially more in May than in January. Parts of the eastern Philippines, the east coast of the Malay Peninsula, and the west Pacific, receive higher amounts of rain in January compared to May.





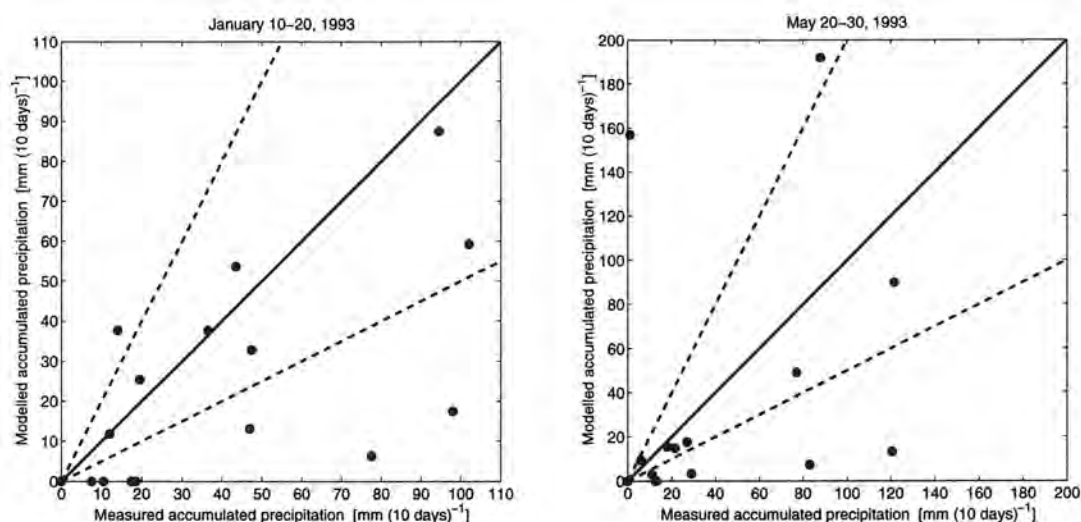
**Figure 5.** Total accumulated precipitation in MATCH domain (sum of 4×31 ECMWF’s 6 hour “First guess”). Top is January 1993, bottom is May 1993. Also displayed are the locations of a few monitoring stations in East Asia.

Figure 6 shows modelled and measured accumulated precipitation in the MATCH domain, at most of the stations in Fig. 5 for a 10 day period in January and May, respectively. There is a considerable scatter around the 1:1 line and it appears that the forecasts often underestimate the precipitation compared to measurements. It should be noted, however, that while inputting precipitation to MATCH, a “limiter” is applied to filter out spurious small precipitation amounts that tend to occur in the meteorological driver and which have a profound effect on the wet deposition calculations.

$$P_{MATCH} = \begin{cases} 0.0 & P < P_{limit} \\ P_{driver} & P \geq P_{limit} \end{cases} \quad (17)$$

In this application we have chosen  $P_{limit}$  to be  $0.5 \text{ mm h}^{-1}$ . Further down in this report we will show that the model has a tendency to overestimate atmospheric concentrations and underestimation the surface depositions, using a lower value on  $P_{limit}$  would probably rectify some of these problems.

Finally, it is also clear that a 6 hour forecast (such as the “First guess”) is not the optimal description of the precipitation in the area. A longer forecast (to eliminate “spin-up” problems) or, better, an analysis based on observations in the area would have been preferred. However, both of these preferred solutions require the extraction of new meteorological fields and considerable pre-processing of the precipitation data, which was considered beyond the scope of this study.



**Figure 6.** Scatter plot of accumulated precipitation at a few stations in the MATCH domain for 10 days in January and May 1993. Note the different scales on the axes of the two panels. Precipitation data from CRIEPI<sup>1</sup> (Hayami et al., 1999).

#### 4.2 Emissions

Figure 7 shows the modelling domain and the anthropogenic and volcanic sulphur emissions used as input to the dispersion calculations. The emissions originally come on a  $1^\circ \times 1^\circ$  latitude-longitude grid centred on half degrees, which is the requested geometry of the meteorological data; no further spatial interpolation of the emissions is thus required. The area emissions were introduced at the lowest model layer, the large point sources into layer 3, and the volcanic sulphur sources into layer 6, see Table 6. No plume rise calculations, or tracing of the sub-grid plume from large point sources were performed, since the emission inventory did not include the relevant information for such calculations, this is, however, possible in MATCH, and recommended to avoid unrealistically high depositions near the point sources. In all 3 inventories 95 % of the sulphur were assumed to be in the form of  $\text{SO}_2$ ; the rest as sulphate (Carmichael et al., 2000). No seasonality was applied – all emissions were assumed to be constant both over the year and over the day in the present study.

**Table 6.** Amount and height of the sulphur emissions in the Task A and B calculations.

| Source              | Amount emitted<br>( $\text{Tg S year}^{-1}$ ) | Model layer | Approximate height<br>over surface (m) |
|---------------------|---|-------------|--|
| Area sources        | 11.98   | 1           | 0-60                                   |
| Large point sources | 2.43  | 3           | 240-500                                |
| Volcanic sources    | 0.63  | 6           | 1200-1600                              |
| Sum of emissions    | 15.04   |             |  |

#### 4.3 Boundary conditions

The domain was initiated with zero  $\text{SO}_2$  and sulphate at start; no influx of tracer through the boundaries occurred. Sensitivity tests (not shown) confirm that the surface deposition and atmospheric concentration in the lowest model layers vary only little if we instead assign realistic values on the boundaries, and in the domain, at start. The relevant model parameters are summarised in Tables 2-6.

<sup>1</sup> Central Research Institute of Electric Power Industry, Komae City, Japan.

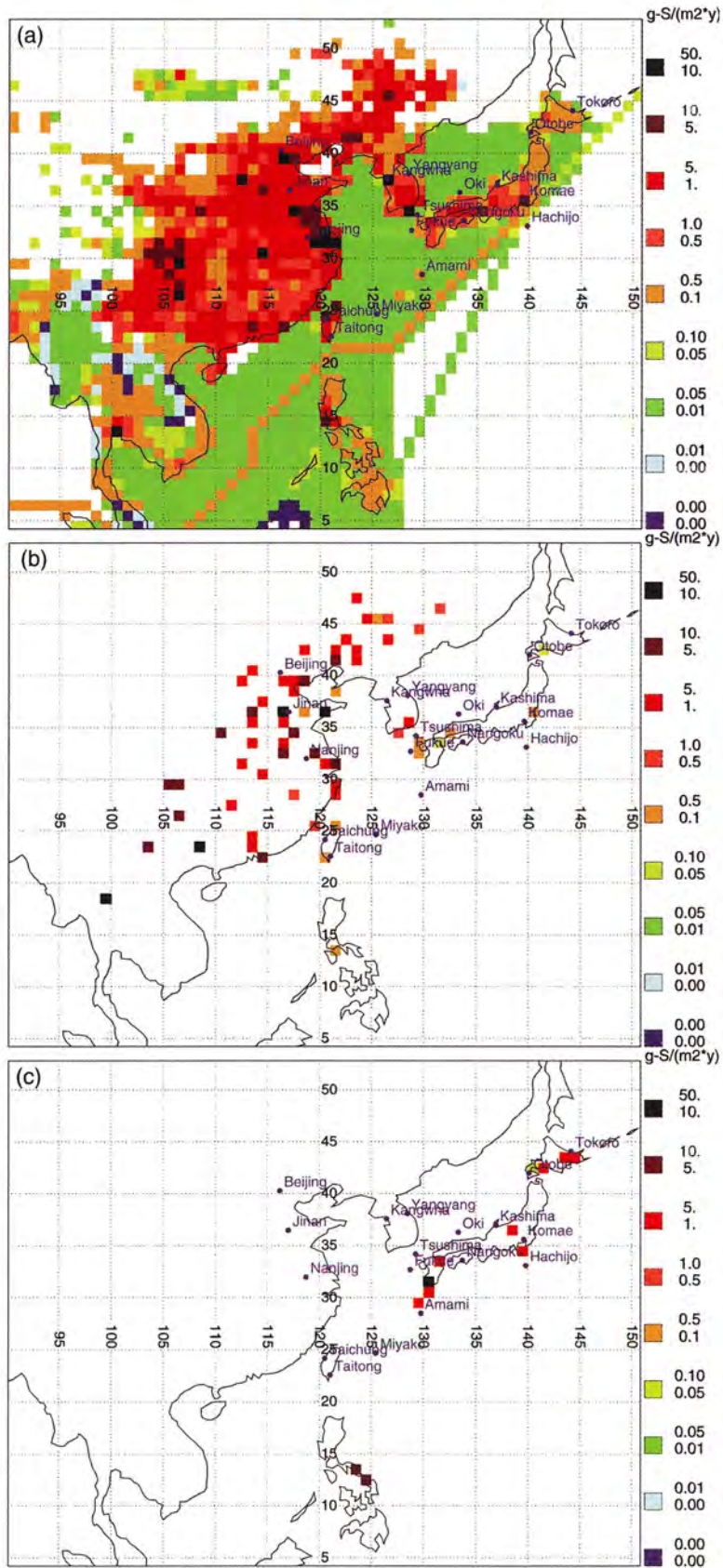


**Figure 7.** Sulphur emissions in the MATCH model domain. (a) is area sources; (b) is large point sources; (c) is volcanic sources. Dark blue is 0.001-0.005, light blue 0.005-0.010  $\text{g S m}^{-2} \text{ year}^{-1}$  etc. The locations of some East Asian measurement stations are also shown. Data from David Streets and the intercomparison community (Carmichael et al., 2000; Streets and Waldhoff, 1999)

## 5. Results

### 5.1 Monthly-mean horizontal distribution

Figure 8 shows near-surface, monthly mean, SO<sub>2</sub> mixing ratio and total sulphate concentration, monthly accumulated dry and wet deposition using Task A parameters for January 1993.

The near-surface concentration/mixing ratio of species  $j$  is deduced from the concentration/mixing ratio in the lowest model layer times the “stability factor”  $F_{stab}^j$  (cf. Eq. 3),

$$\mu_{near-surface}^j = \mu_1^j F_{stab}^j \quad (18)$$

Due to the coarse resolution and the large spatial scale, the horizontal distribution of SO<sub>2</sub> and total sulphate resemble the emission fields quite well. SO<sub>2</sub> and sulphate also show a great deal of similarity although sulphate has a smoother distribution. Over remote areas – like the west Pacific – total sulphate concentrations (in ppb(v)) are higher than SO<sub>2</sub>, while closer to the sources, SO<sub>2</sub> is always higher. This, of course, reflects the longer residence time of sulphate and that it is a secondary pollutant, formed from SO<sub>2</sub>. The largest values of both species occur in the high emission areas in eastern China (i.e. the Sichuan province, (Chengdu, Chongqing, etc.), and in the densely populated Yellow River basin), and over the large cities in the region (Bangkok, Manila, Seoul, Pusan, etc.). Monthly mean SO<sub>2</sub> mixing ratios reach 5-10 ppb(v), or more, over substantial areas of eastern China and South Korea, and 2-5 ppb(v) over southern Japan and the rest of eastern China and Korea. Monthly-mean total sulphate concentrations reach over 2 µg S m<sup>-3</sup> over most of eastern China.

While the dry deposition mirrors the atmospheric concentration of SO<sub>2</sub> and sulphate, the wet deposition is strongly modulated by the precipitation. Hence it has a much more patchy appearance. Maximum wet depositions – of several 100 mg S m<sup>-2</sup> month<sup>-1</sup> – occur both in the high emission areas in e.g. eastern China, and in areas with high precipitation rates, e.g. east side of the Malay Peninsula.

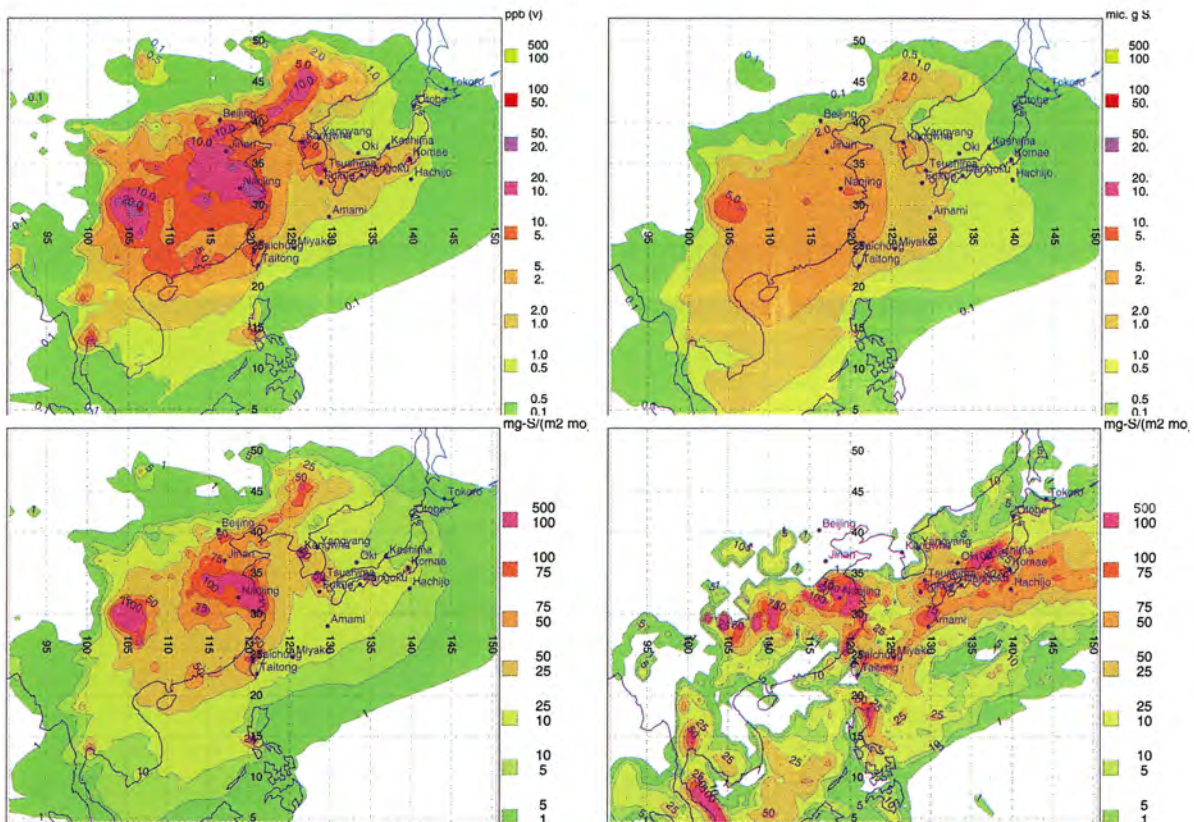


**Figure 8.** Modelled January 1993 sulphur concentration and depositions. (upper left) is near-surface, monthly mean SO<sub>2</sub> mixing ratio (ppb(v)); (upper right) is near-surface, monthly mean, total sulphate concentration ( $\mu\text{g S m}^{-3}$ ); (lower left) is accumulated dry deposition ( $\text{mg S m}^{-2} \text{ month}^{-1}$ ); (lower right) is accumulated wet deposition ( $\text{mg S m}^{-2} \text{ month}^{-1}$ ).

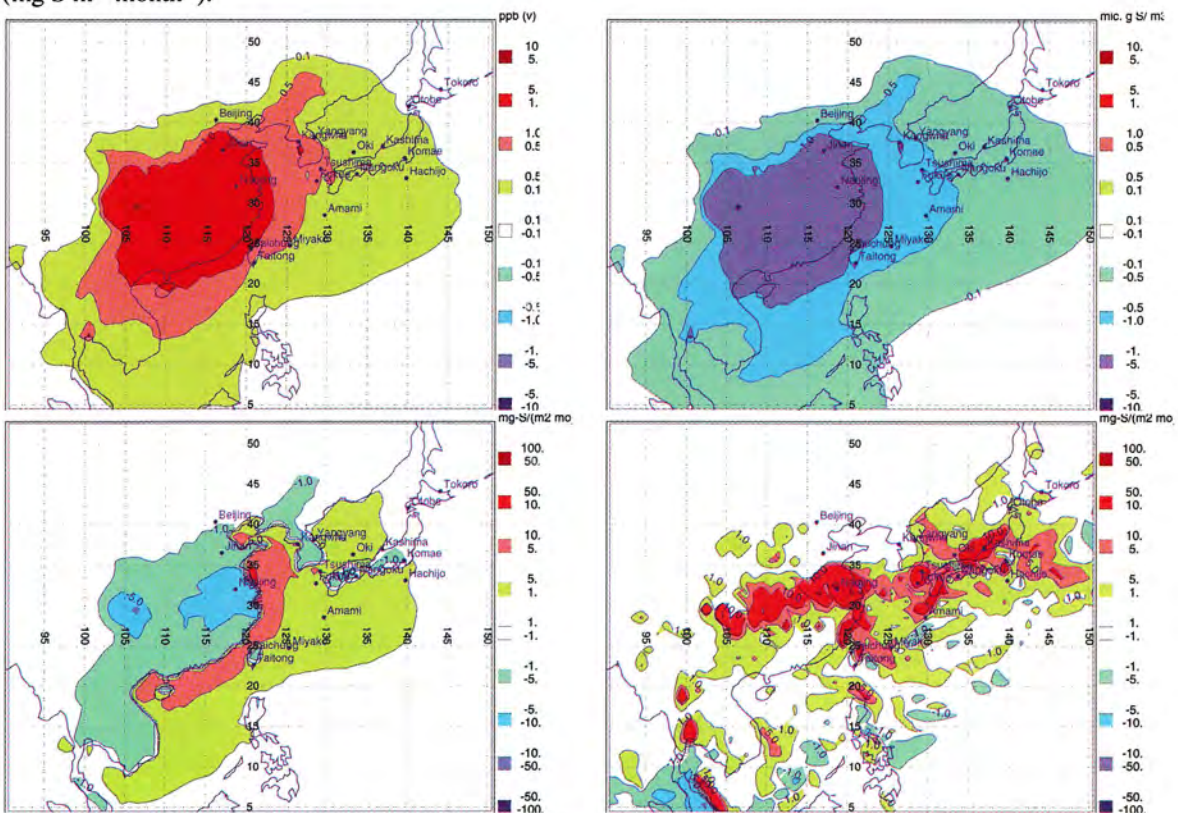


**Figure 9.** Difference between Task A and Task B results in January 1993. (upper left) is near-surface monthly mean SO<sub>2</sub> mixing ratio (ppb(v)); (upper right) is near-surface, monthly mean, total sulphate concentration ( $\mu\text{g S m}^{-3}$ ); (lower left) is accumulated dry deposition ( $\text{mg S m}^{-2} \text{ month}^{-1}$ ); (lower right) is accumulated wet deposition ( $\text{mg S m}^{-2} \text{ month}^{-1}$ ).

Figure 9 shows the difference in result between Task A and B parameters. Due to the slower SO<sub>2</sub> to sulphate conversion in Task A (cf. Fig. 4), SO<sub>2</sub> is higher and sulphate lower in the standard (Task A) simulation.

Because the dry- and wet- depositions are the sum of SO<sub>2</sub> and sulphate depositions, there are some peculiar effects in Fig. 9, with alternating areas of increasing and decreasing depositions. Although dry deposition of SO<sub>2</sub> dominates over sulphate in the complete domain (cf. Table 7, 8) there is a larger absolute decrease in sulphate dry deposition over the emission areas when using Task B parameters. The largest absolute increase in SO<sub>2</sub> dry depositions using Task B parameters occur immediately downwind the emission areas, i.e. in the China Sea just off the Asian continent. Hence the bi-polar feature of the change in accumulated dry deposition shown in Fig. 9. Most areas have higher wet deposition in the standard (Task A) simulation, due to the more efficient wet scavenging compared to Task B (cf. Fig. 3). There are, however, some areas with less wet deposition – a competing effect from the lower sulphate amounts that is present in the Task A simulation.

The difference in results between the Task A and B simulation are not very substantial in terms of concentrations and depositions, although the conversion rate and the scavenging rate differs by at least a factor of 2. At this stage we judge the uncertainty in emission inventory, and driving meteorology, much larger than the uncertainty in the model parameters. Further down, we will also show several examples of the ambiguity of choosing a representative value at a particular measurement station, which will also be an additional uncertainty when verifying model results against observations.

Figure 10 shows near-surface, monthly mean atmospheric concentration and deposition of SO<sub>2</sub> and sulphate for May, 1993.

The SO<sub>2</sub> to sulphate conversion rate is faster in May than in January (cf. Fig. 4). However, both SO<sub>2</sub> and total sulphate show lower values in May compared to January, due to the more effective dry- (cf. Table 2), but in particular, wet- (cf. Fig. 5 showing precipitation intensity) deposition of both species. In May, large connected areas of eastern China have sulphur wet deposition in excess of 100 mg sulphur m<sup>-2</sup> month<sup>-1</sup>. The modelled dry deposition is well over 25 mg sulphur m<sup>-2</sup> month<sup>-1</sup> in eastern China, Korea and parts of Japan for both January and May, 1993.

Figure 11 shows the difference between Task A and B parameters for the May, 1993 simulations. The shorter atmospheric residence times of sulphuric species in May are visible in the smaller absolute differences between the 2 simulations.

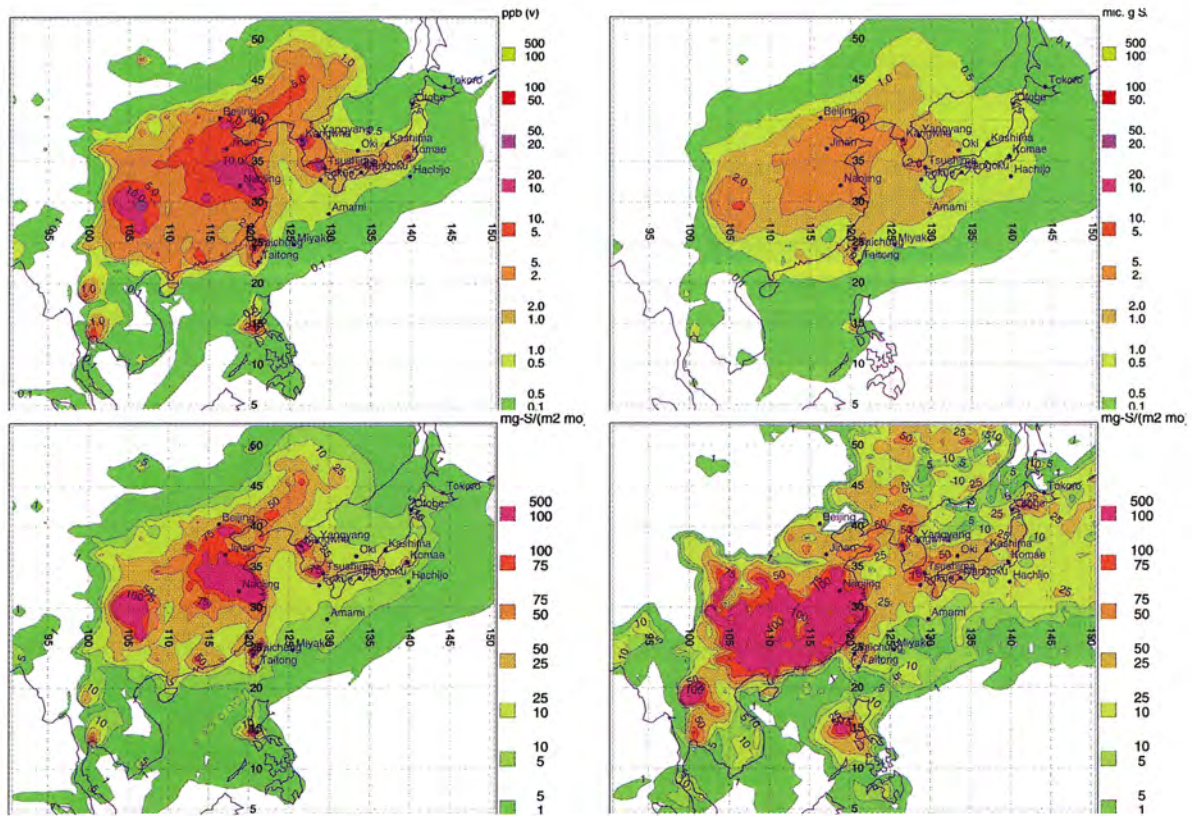


Figure 10. As Fig. 8 but for May 1993.

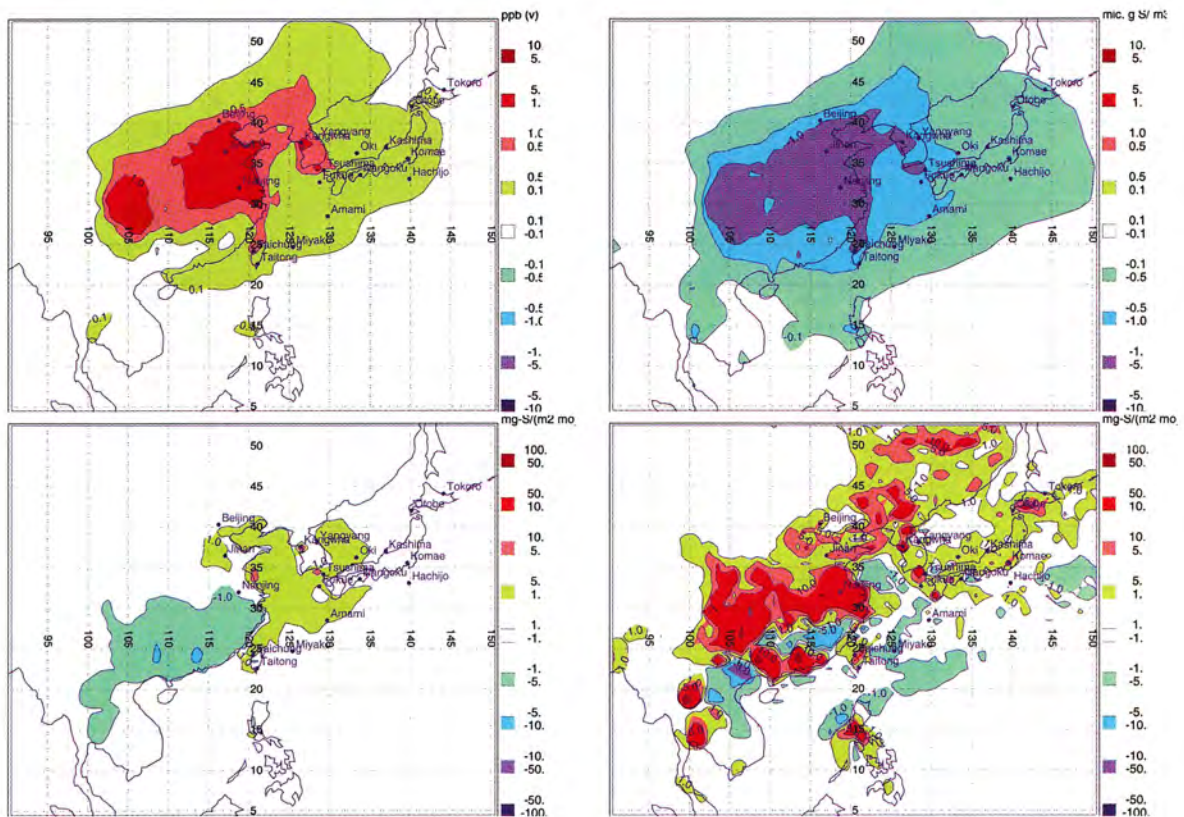
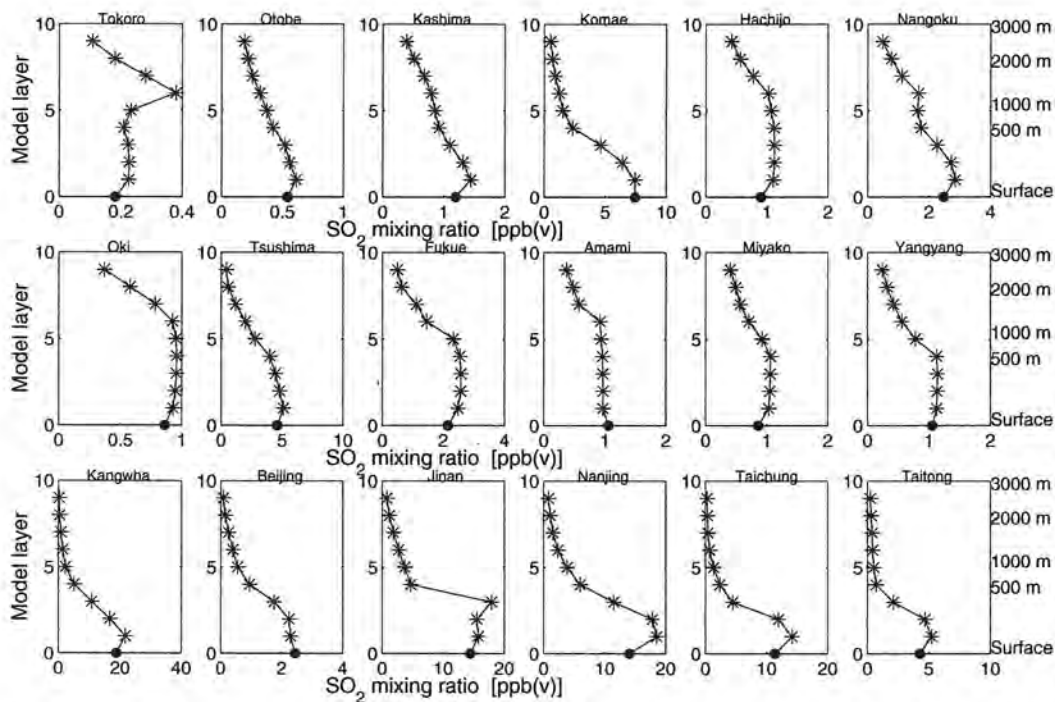


Figure 11. As Fig. 9 but for May 1993.

### 5.2 Monthly-mean vertical profiles, Task A parameters

Figures 12-15 show vertical profiles of SO<sub>2</sub> and total sulphate over a number of stations in the modelling domain using the standard (Task A) parameters. The figures also illustrate the difference between near-surface and lowest model layer mixing ratio (cf. Eq. 18). The data plotted are monthly mean values at the respective model layer and monthly mean near-surface values. The near-surface mixing ratio is always lower than the mixing ratio in the lowest model layer but since the reduction is dependent on the local stability and surface type, the magnitude will differ from site to site.

For some stations the near-surface mixing ratio seems to be equal or higher than in the lowest model layer. This is, however, an artefact of the averaging procedure. The near-surface value is a true monthly mean, while the model layer means are constructed from the 00:00 GMT values (which is local morning for the East Asian stations) and may thus be skewed towards lower values.



**Figure 12.** SO<sub>2</sub> mixing ratio (in ppb(v)) for January 1993, in the lowest 9 model layers, and near the surface, over the stations in Fig 7-11. Asterisks are monthly mean values at model layers. Solid dot is monthly mean near-surface value. The monthly mean values on model levels are created from the 31 instantaneous values at 00Z each day of January 1993. The surface values are deduced from the instantaneous value in the lowest model layer times the instantaneous local stability factor  $F_{stab}^j$ , then averaged over all time steps in the model. Approximate heights over surface are also indicated to the right of the panels.

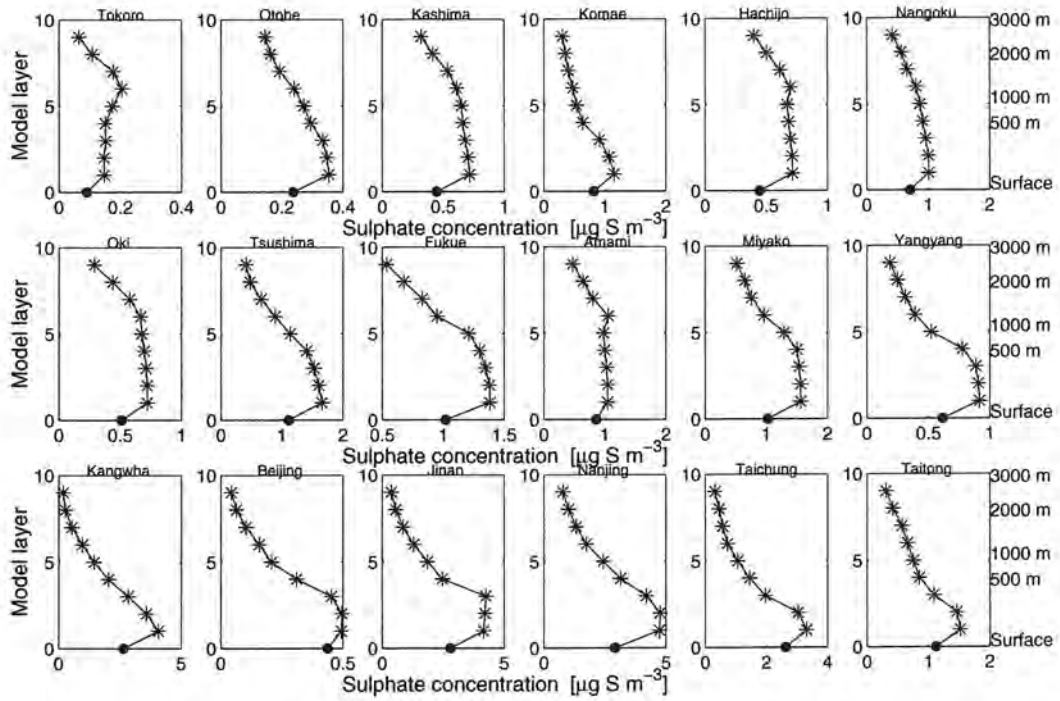


Figure 13. As Figure 12, but total sulphate (in  $\mu\text{g S m}^{-3}$ ).

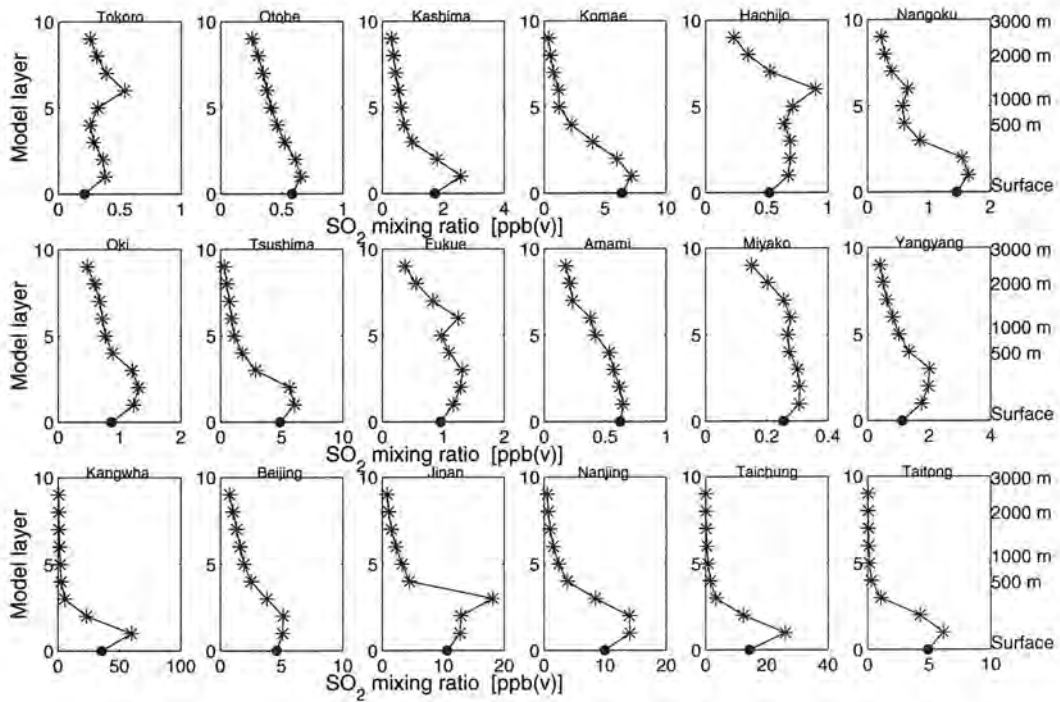


Figure 14. As Figure 12, but for May 1993.

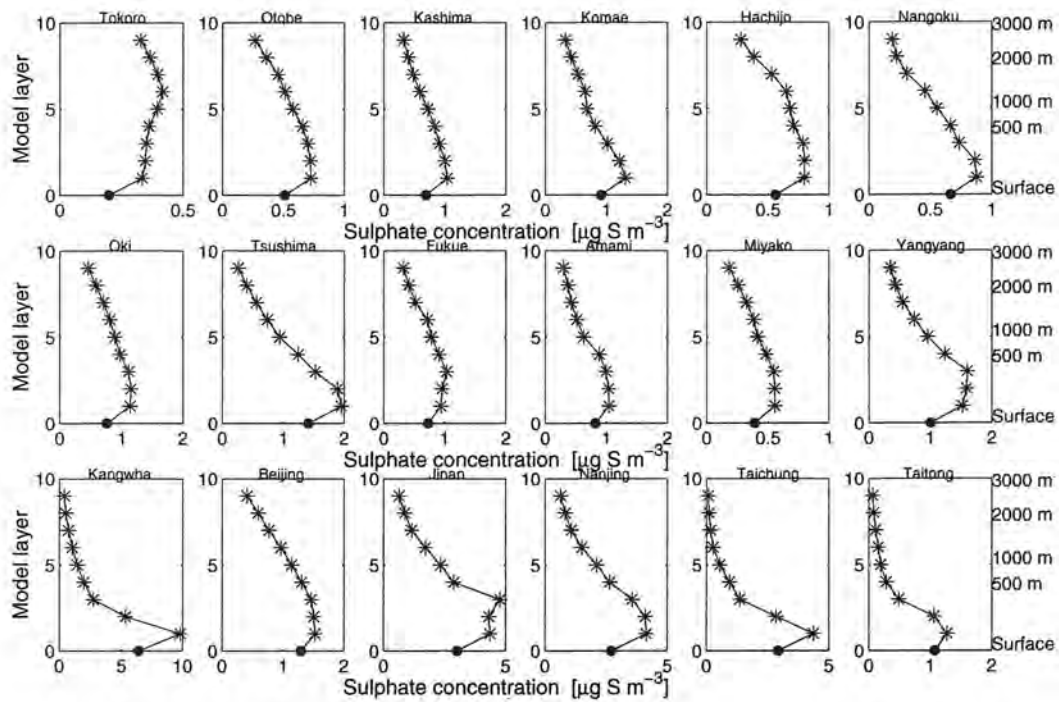


Figure 15. As Figure 13, but for May 1993.

Although the profiles in Fig. 12-15 are smoothed out during the construction of the monthly mean, they still contain interesting pieces of information. A clear influence from the large point sources (emitting directly into layer 3, cf. Fig. 7b) can be seen, in both  $\text{SO}_2$  and total sulphate, over e.g. Jinan during both months. The volcanic influence (cf. Fig 7c) is smaller, but is visible in the  $\text{SO}_2$  profile over Tokoro during both months and over Hachijo and Fukue in May.

Kangwha, north of Seoul, lies in a gridbox with high surface emission but no lofted sources, consequently the vertical profile of  $\text{SO}_2$  and total sulphate is very pronounced. For stations away from the sulphur sources (e.g. Tokoro, Hachijo, Oki, Fukue, Amami, Miyako) the vertical variations are much less in the lower troposphere.

### 5.3 Time series, Task A parameters

In order to examine the temporal evolution of the advected species we next present time series of near-surface  $\text{SO}_2$ , total sulphate concentration, and total sulphur deposition.

Figs. 16-21 show the rapid, and large, day-to-day variation in atmospheric concentration and deposition at a numbers of sites. At many stations, the daily mean atmospheric concentration varies over an order of magnitude, see e.g. Tsushima, Fukue, Beijing, Nanjing. The variation in atmospheric concentration is mostly a factor of local wind direction while the episodic character of the rain determines the timing of the wet deposition. Long periods without rain are interrupted with an occasional rain shower, which causes significant deposition at that date.

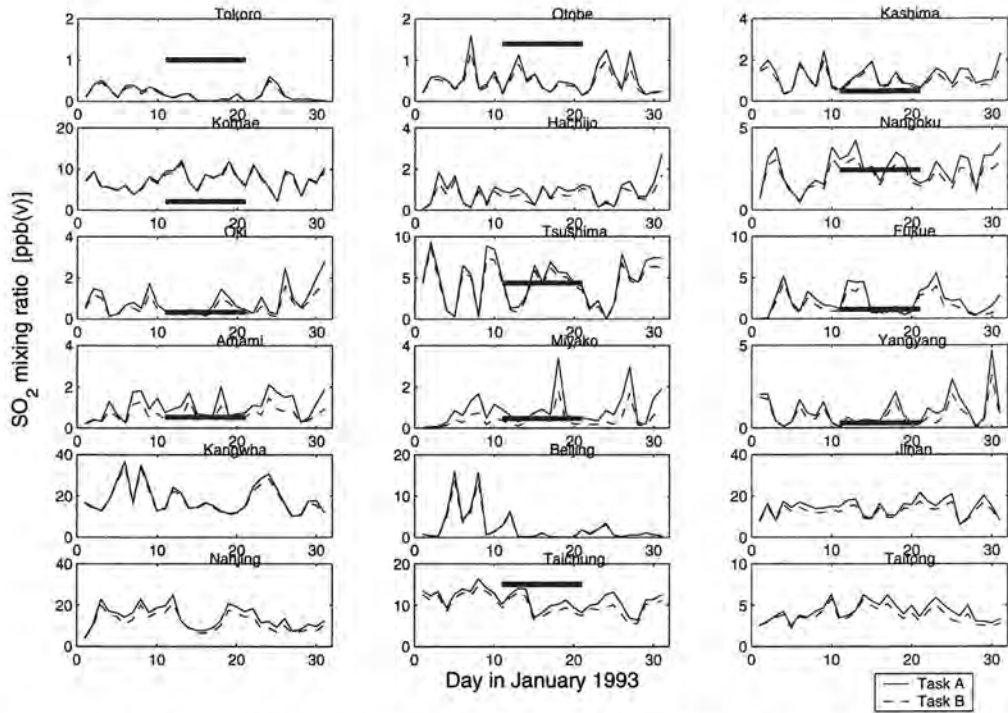


**Figure 16.** Time series of modelled, daily mean, near-surface  $\text{SO}_2$  (ppb(v)) at the East Asian stations shown in Fig. 7-11 during January 1993. Solid line is standard (Task A) simulation, dashed line is Task B simulation. Thick horizontal line is 10-day average from measurements collected at the respective station. Sulphur measurements from CRIEPI (Hayami et al., 1999).

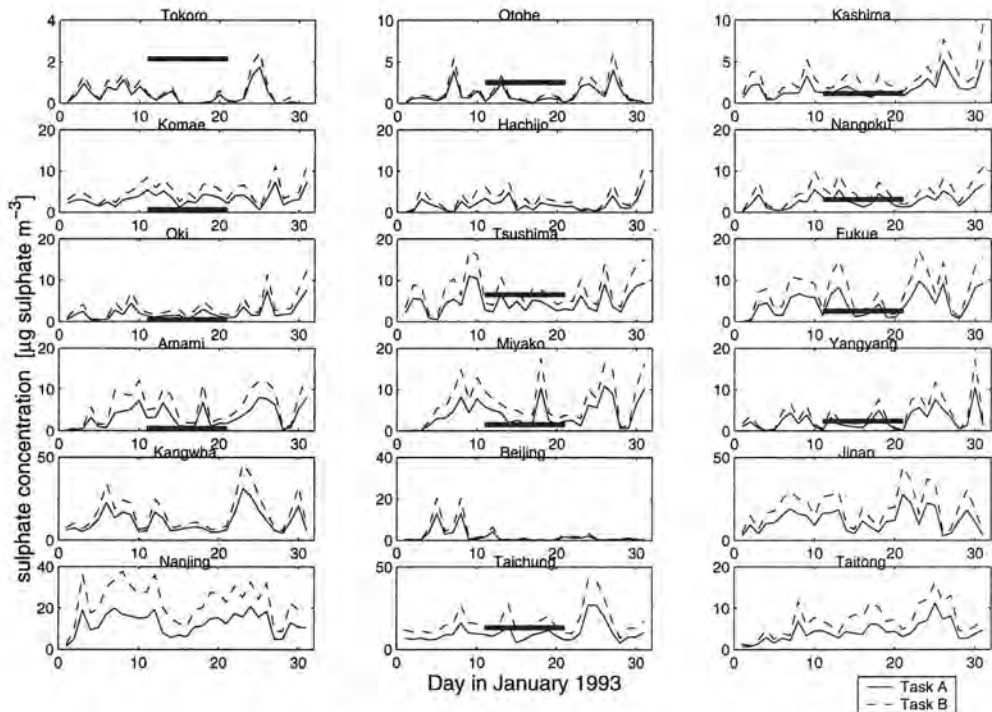


**Figure 17.** As Fig. 16 but for total sulphate concentration ( $\mu\text{g SO}_4^{2-} \text{m}^{-3}$ ).

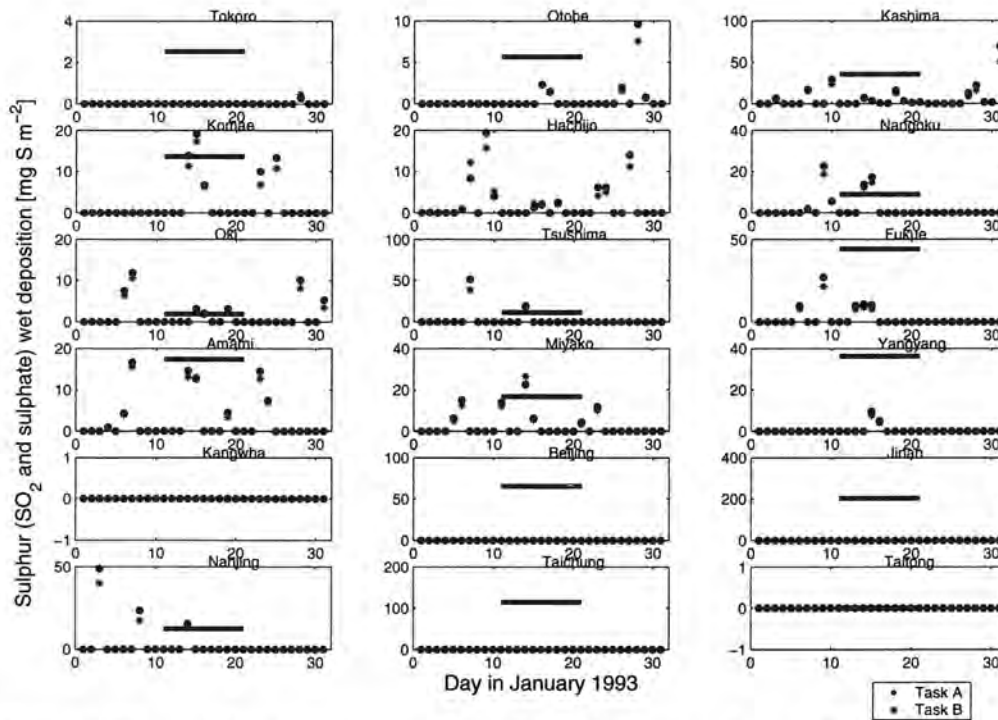


**Figure 18.** Total ( $\text{SO}_2$  + sulphate) wet deposition at the East Asian stations shown in Fig. 7-11 during January, 1993. Dots are standard (Task A) parameters, asterisks, Task B parameters (both in  $\text{mg S m}^{-2} \text{ day}^{-1}$ ). Thick horizontal line is 10-day accumulated wet deposition from measurements collected at the respective station ( $\text{mg S m}^{-2} (10 \text{ days})^{-1}$ ). Deposition measurements from CRIEPI (Hayami et al., 1999).

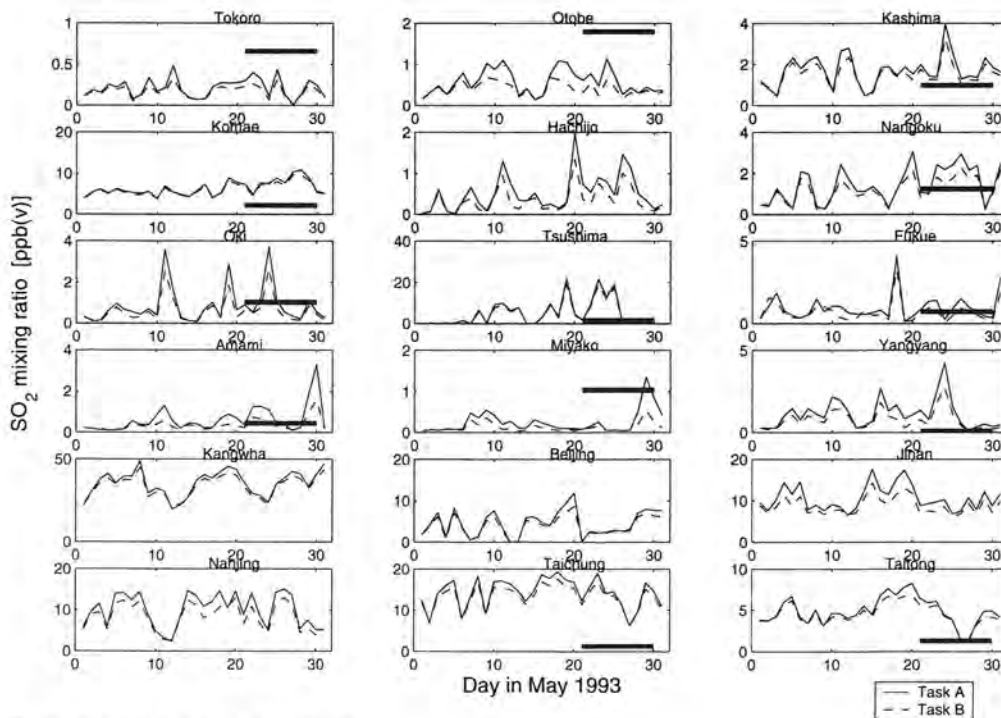


**Figure 19.** As Fig. 16 but for May, 1993.

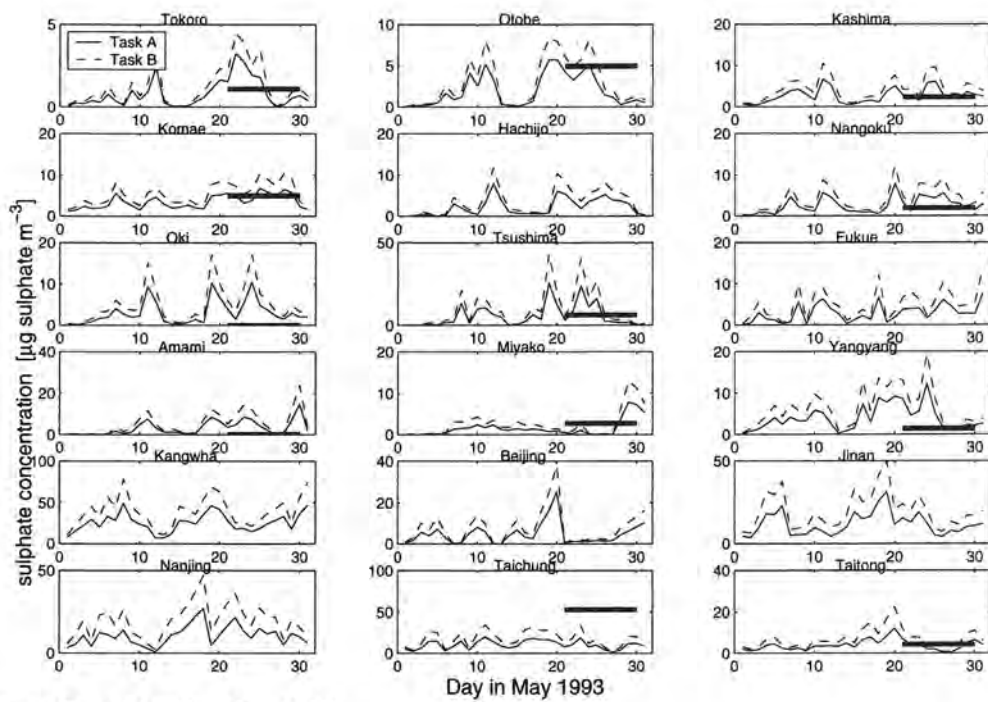


Figure 20. As Fig. 17 but for May, 1993.

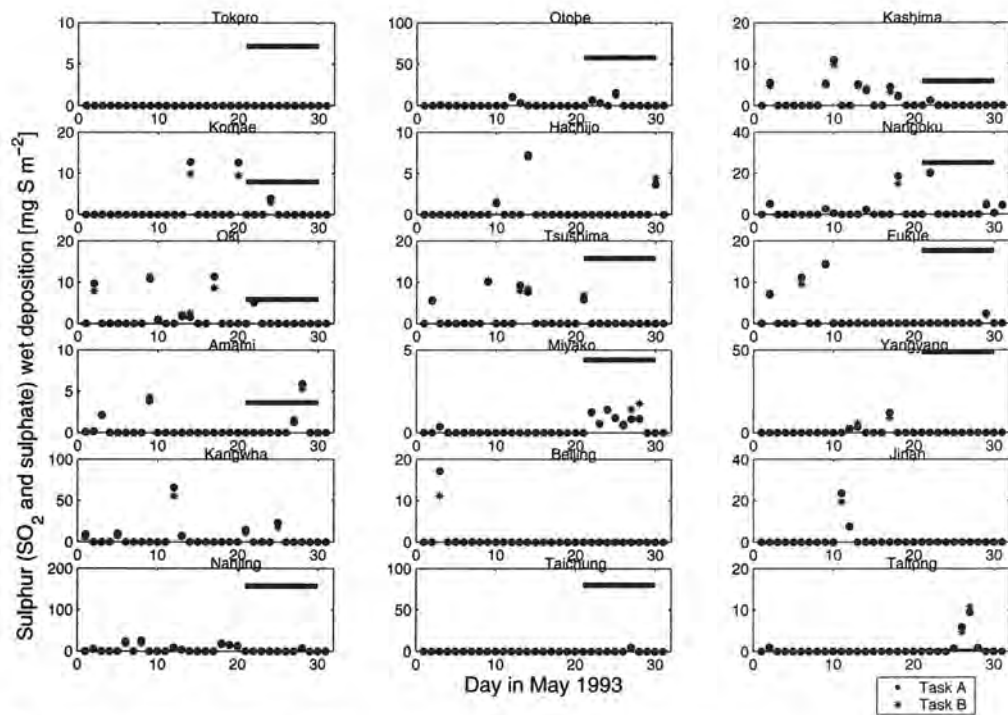


Figure 21. As Fig. 18 but for May, 1993.

For several stations there is a significant over- (or under-) estimation of the 10-day mean values in the model, compared to measurements. This can, of course, point towards errors in the transport model, emission inventory, driving meteorology, or simply that the monitoring station is not representative for the 1°×1° gridbox that the model results represent.

Figs. 16-21 again illustrate the small difference in results between the Task A and task B simulation. Of course SO<sub>2</sub> is systematically higher in Task A and sulphate higher in Task B, but the natural day-to-day variability is much larger than the difference between Task A and B results. It is interesting to note that the diurnal variations at a site are very similar in the two experiments. Both for remote stations and for stations near the emissions, the difference is almost only a parallel shift of the values up or down.

#### 5.4 Comparison with measured data, Task A parameters

In Figures 12-21 we have plotted the modelled value in the gridbox containing the measurement station in question. In areas of large horizontal gradients such a method is probably not optimal, see Fig. 22 which illustrates this feature.

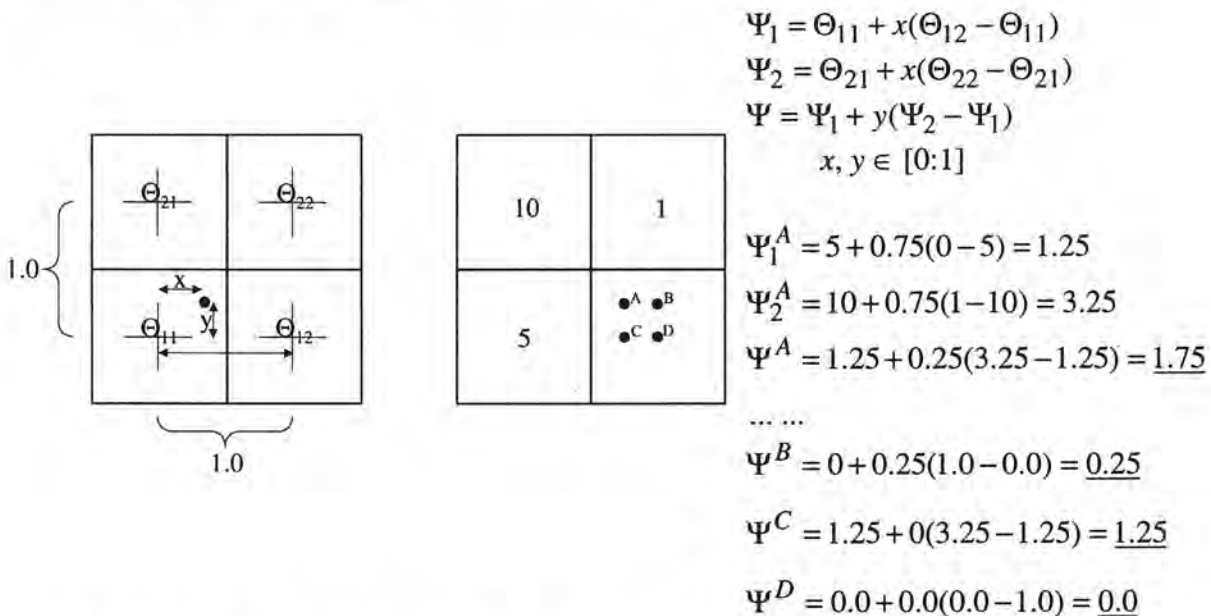


**Figure 22.** Principle of “bilinear interpolation”, and a numerical example. The left figure and the top 4 equations outline the mathematics. The right figure shows 4 monitoring stations at locations A, B, C, D. The monitoring stations lie in a cell with  $\Psi = 0$ , while neighbouring cells have 10, 1, and 5. In a conventional, “nearest gridpoint”, extraction all 4 stations would get  $\Psi = 0.0$ , using bilinear interpolation, the values range from 0.0 to 1.75 and local gradient becomes clear.

In Figs. 23-26, we have plotted the 10-day mean value of modelled concentration vs. measurement for the stations where there is available data (cf. Figs. 16-21). We display the results from Task A and Task B simulation in the gridbox where the respective monitoring station is located (“nearest gridpoint”). For the Task A simulation, we also display the “bilinearly interpolated” value (cf. Fig. 22). As can be seen, the difference between nearest gridpoint and bilinearly interpolated data is often larger than the difference between the 2 sets of model parameters!

Apart from this interesting finding, we note that, for January, the model performs reasonably well with regards to the 10-day mean measured  $\text{SO}_2$  mixing ratio at the available stations. It slightly overestimates atmospheric total sulphate concentration, especially with Task B parameters, and severely underestimates sulphur wet deposition at a few stations without precipitation. This latter mismatch between data and modelled results should, however, not be attributed to the MATCH model, rather to the large-scale meteorological driver, which fails to prescribe precipitation at this location (cf. Fig. 6). Noteworthy is that this failure persistently occurs at the stations that report the highest wet deposition amounts. The reason for this feature is unclear.

For May, the model seems to overestimate both  $\text{SO}_2$  and total sulphate, and again, totally miss the wet deposition at a number of sites. The overestimation of atmospheric total sulphate is, again, more severe in the Task B simulation. The different formulations of oxidation and wet scavenging are expected to result in significantly higher sulphate concentrations in Task B, since the sulphate production is more effective and the wet scavenging less effective. For  $\text{SO}_2$ , the difference should be much smaller, since the effects of the different formulations act in opposite directions and roughly cancel out.

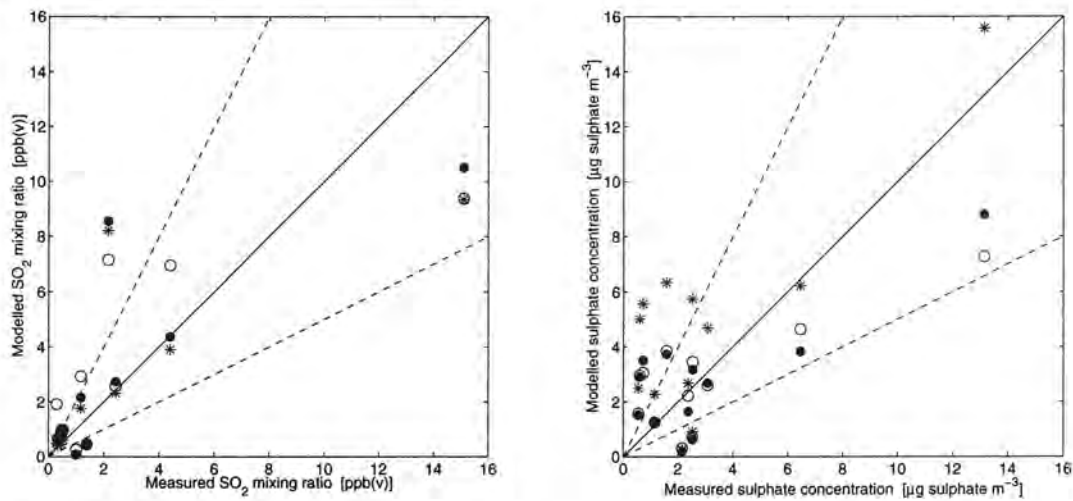


**Figure 23.** Modelled  $\text{SO}_2$  and total sulphate 10-day mean concentrations vs. measurements for January 11-21, 1993. Dots and circles are Task A parameters; asterisks are Task B parameters. The dots and the asterisks are the values in the gridbox containing the measurement station. The circles are constructed from a bilinear interpolation of neighbouring gridboxes (from the very same (Task A) data set as the solid dots!). Sulphur measurements from CRIEPI (Hayami et al., 1999).

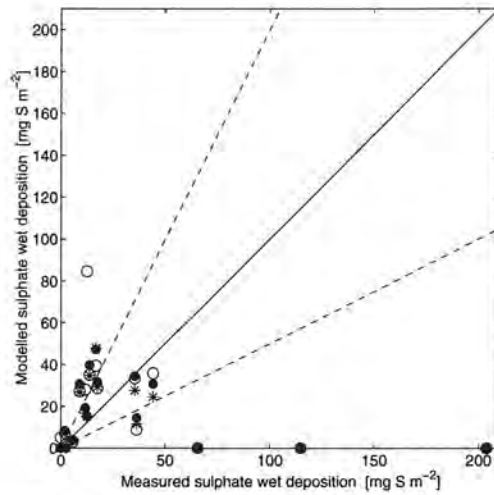


**Figure 24.** 10-day accumulated modelled vs. measured total sulphate ( $\text{SO}_2 + \text{SO}_4^{2-}$ , see Eq. (5)) wet deposition for January 11–21, 1993. Dots and circles are Task A parameters; asterisks are Task B parameters. The dots and the asterisks are the values in the gridbox containing the measurement station. The circles are constructed from a bilinear interpolation of neighbouring gridboxes (from the very same (Task A) data set as the solid dots!). Deposition measurements from CRIEPI (Hayami et al., 1999).

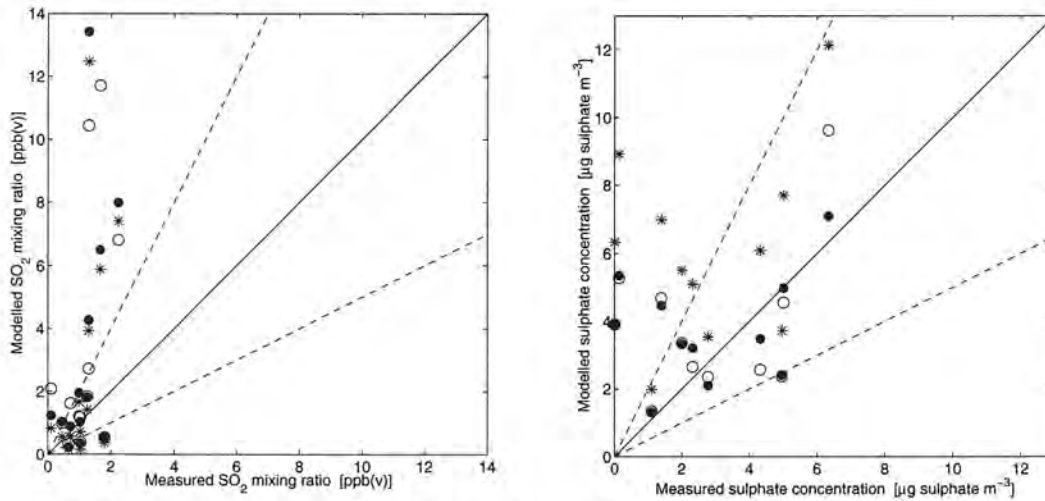


**Figure 25.** As Fig. 23 but for May 21–30, 1993. (Taichung with a reported measured sulphate concentration of  $53 \mu\text{g sulphate m}^{-3}$  is omitted in the plot).

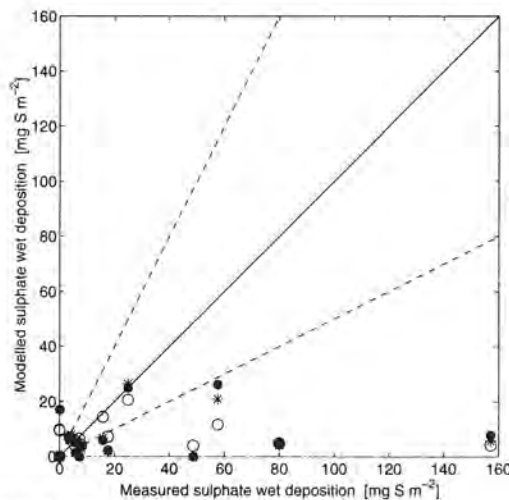


**Figure 26.** As Fig. 24 but for May 21–30, 1993.

### 5.5 Budget values

Above, we have shown many examples on the relatively small difference in atmospheric concentration and deposition using various numerical values on chemical conversion and wet scavenging. The difference between the Task A and Task B simulation was shown to be much less than the natural day-to-day variation, which is governed by the driving meteorology. If we instead examine the sulphur reservoirs and the gross fluxes in the model, we note considerable discrepancies between the two configurations. The differences between the Task A and Task B results are summarised in Tables 7 and 8.

**Table 7.** Budget terms for the sulphur simulations covering January 1993, using the standard (Task A) parameters and the prescribed (Task B) parameters. The mass is the instantaneous mass at end of simulation, the other values are accumulated over the whole 31 day simulation.

|  |        | SO <sub>2</sub> | Sulphate |
|--|--------|-----------------|----------|
| Mass in domain at end of simulation (10 <sup>9</sup> g S)            | Task A | 77.6            | 61.8     |
|  | Task B | 46.4            | 96.5     |
| Total emission (10 <sup>9</sup> g S month <sup>-1</sup> )            | Task A | 1213.6          | 63.9     |
|  | Task B | 1213.6          | 63.9     |
| Total outflow (10 <sup>9</sup> g S month <sup>-1</sup> )             | Task A | 147.5           | 182.5    |
|  | Task B | 72.6            | 303.0    |
| Total dry deposition (10 <sup>9</sup> g S month <sup>-1</sup> )      | Task A | 296.6           | 99.3     |
|  | Task B | 228.4           | 162.6    |
| Total wet deposition (10 <sup>9</sup> g S month <sup>-1</sup> )      | Task A | 181.3           | 230.9    |
|  | Task B | 69.3            | 298.7    |
| Total chemical conversion (10 <sup>9</sup> g S month <sup>-1</sup> ) | Task A | 510.6           |          |
|  | Task B | 796.9           |          |
| Turnover time (days)   | Task A | 2.4             | 5.8      |
|  | Task B | 1.3             | 6.5      |

**Table 8.** Same as Table 7, but for May 1993.

|  |        | SO <sub>2</sub> | Sulphate |
|--|--------|-----------------|----------|
| Mass in domain at end of simulation (10 <sup>9</sup> g S)            | Task A | 55.8            | 52.6     |
|  | Task B | 33.7            | 85.1     |
| Total emission (10 <sup>9</sup> g S month <sup>-1</sup> )            | Task A | 1213.6          | 63.9     |
|  | Task B | 1213.6          | 63.9     |
| Total outflow (10 <sup>9</sup> g S month <sup>-1</sup> )             | Task A | 117.2           | 162.1    |
|  | Task B | 55.1            | 263.2    |
| Total dry deposition (10 <sup>9</sup> g S month <sup>-1</sup> )      | Task A | 286.6           | 60.9     |
|  | Task B | 242.2           | 106.0    |
| Total wet deposition (10 <sup>9</sup> g S month <sup>-1</sup> )      | Task A | 325.7           | 216.6    |
|  | Task B | 171.9           | 320.2    |
| Total chemical conversion (10 <sup>9</sup> g S month <sup>-1</sup> ) | Task A | 428.3           |          |
|  | Task B | 710.6           |          |
| Turnover time (days)   | Task A | 1.7             | 5.9      |
|  | Task B | 0.9             | 6.2      |

Due to the very efficient wet scavenging in our model, and the higher precipitation amounts in May compared to January, the sink processes for sulphuric species are more efficient during May. Hence, the total mass of SO<sub>2</sub> and sulphate are both higher in January, compared to May. Task B has a faster SO<sub>2</sub> to sulphate conversion rate, therefore is the SO<sub>2</sub> burden always lower and sulphate always higher using Task B parameters. In the Task B set-up, the total mass of sulphur as sulphate always exceed the SO<sub>2</sub>-sulphur with more than a factor of 2, while for the Task A simulation there is a slight excess of SO<sub>2</sub>-sulphur.

In the Task B simulation, the dry deposition of sulphate increases proportionally more than the wet deposition compared to the standard (Task A) simulation. Simultaneously, the wet deposition of SO<sub>2</sub> decreases proportionally more. This illustrates the effect of the different formulation of wet scavenging between in Task A and Task B (Task B has a much less effective wet scavenging of SO<sub>2</sub> and sulphate).

Neglecting the fluxes across the model boundaries, the turnover time for SO<sub>2</sub> and sulphate,  $\tau^j$ , can be defined as:

$$\tau^{SO_2} = \frac{M^{SO_2}}{D^{SO_2} + W^{SO_2} + C^{SO_2}}, \quad (19a)$$

$$\tau^{SO_4^{2-}} = \frac{M^{SO_4^{2-}}}{D^{SO_4^{2-}} + W^{SO_4^{2-}}}, \quad (19b)$$

where  $M^j$  is the mass at the end of simulation (which is close to the average mass of species  $j$  over the whole simulation period).  $D^j$ ,  $W^j$ , and  $C^j$ , are the total-, dry, and wet deposition and the chemical destruction respectively.

The turnover times thus calculated are 1-2 days for SO<sub>2</sub> while they are 5-6 days for sulphate. The higher precipitation amounts in May result in shorter turnover times during this time compared to the situation in January.

The more efficient conversion of SO<sub>2</sub> to sulphate using Task B parameters results in a considerably shorter turnover time for SO<sub>2</sub> but a slightly longer turnover time for sulphate using Task B parameters. This is not completely in line with the results in Fig. 23 and Fig. 25 which indicate that near-surface SO<sub>2</sub> is only slightly lower, while near-surface sulphate is considerably higher in the Task B simulation compared to the standard (Task A) simulation. The reason for this is unclear.

### 5.6 Source-receptor calculations, Task A parameters

Finally, an attempt was made to attribute the total deposition at a number of sites to specific source regions. The land-based anthropogenic sulphur emissions in Figs. 7a,b were divided into 8 regions, as shown in Table 9 and Fig. 27. The volcanic sulphur sources in Fig 7c were treated as a separate region see Table 9.

**Table 9.** Summary of regional and volcanic emissions. The regional breakdown of the anthropogenic sulphur sources includes both area and large point sources. The sum does not add up to the previous total because the omissions of oceanic sources and the truncation of some coastal sources.

| Region           | Sum of emissions<br>(Tg S yr <sup>-1</sup> ) | Fraction of all emissions<br>(%) |
|------------------|--|----------------------------------|
| Japan            | 0.44   | 3.7                              |
| Korea            | 0.74   | 6.2                              |
| NE China         | 1.15   | 9.6                              |
| C-E China        | 3.60   | 30.0                             |
| S China          | 3.92   | 32.6                             |
| Taiwan           | 0.09   | 0.7                              |
| SE Asia          | 0.66   | 5.5                              |
| NW Asia          | 0.78   | 6.5                              |
| Volcanic         | 0.63   | 5.2                              |
| Sum of emissions | 12.01  | 100.0                            |

The model was run with the standard set-up (Task A parameters), using only one of the 9 inventories at a time, and the total deposition at the stations in Fig. 27 was calculated. The results are summarised in Figs. 28-29.

Of the 7 sites in Figs. 28 and 29, the Chinese station Nanjing, clearly has the highest total deposition, with values around 200 mg S m<sup>-2</sup> month<sup>-1</sup>. Nanjing lies in the region “C-E China” which is the dominating source region at this site. In May, the influence from “S China” is also substantial at Nanjing.

The volcanic influence is clearly visible at several Japanese sites, especially in May.

Yangyang, in Korea, has no influence from the Japanese sources in January but a clear influence in May. This, of course, is a reflection of the variation in the predominant wind directions during the two months.

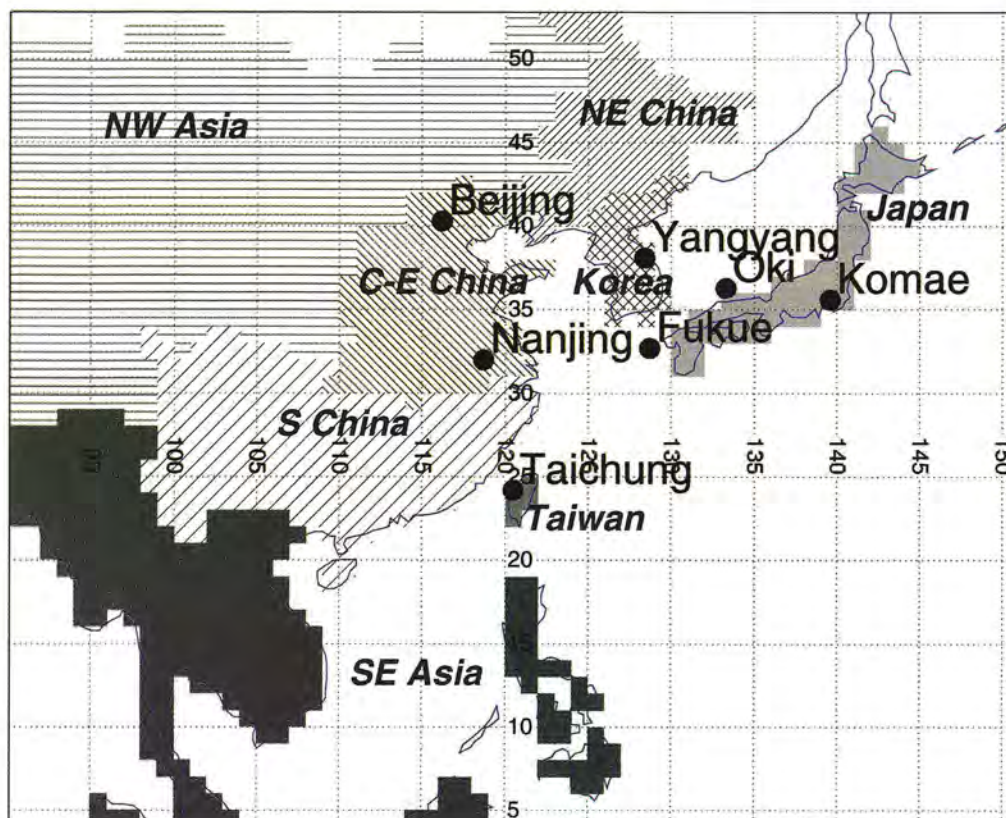


**Figure 27.** The 8 source regions and the 7 stations used in the source-receptor calculations.

For the Japanese station Komae, which lies on the east side of the Japanese mainland, Japanese sources are dominating the deposition. For the stations on the west coast of Japan (Oki, and Fukue), on the other hand, Chinese and Korean emissions are dominating the deposition. In January 80-90 % of the deposition at these sites originates from China and Korea. The corresponding number for May is 40-50 %

Tables 10 and 11 summarise the relative importance of the volcanic and anthropogenic sulphur sources at the 7 sites in Figs. 28 and 29. The results should be taken as, at least, preliminary, and definitely only valid for the two selected periods in 1993. From the large difference between the two months, it is clear that the situation will be different for other months and for other years with different transport and precipitation regimes. Also, since the turnover times for SO<sub>2</sub> and sulphate were shown to be quite different between the Task A and Task B simulations, it should also be expected that the respective contribution from various source regions – at different distances from the receptors – could be quite different using different model parameters.

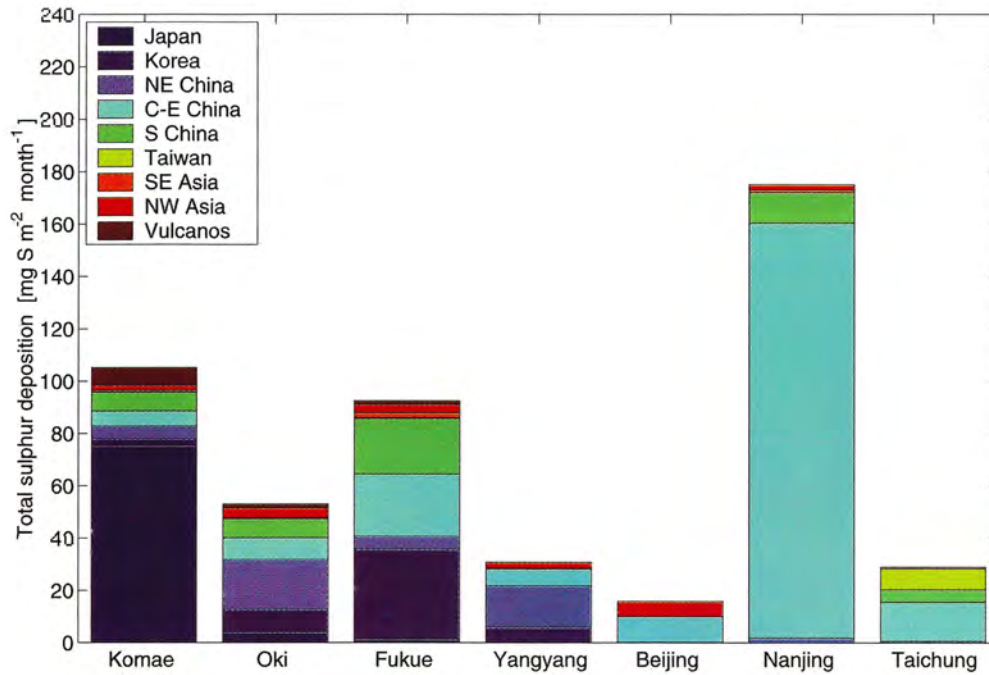


**Figure 28.** Respective contribution to the total sulphur deposition from volcanic and the 8 East Asian regions in Fig. 27 at 7 selected monitoring stations in East Asia for January 1993. Units  $\text{mg S m}^{-2} \text{ month}^{-1}$ .

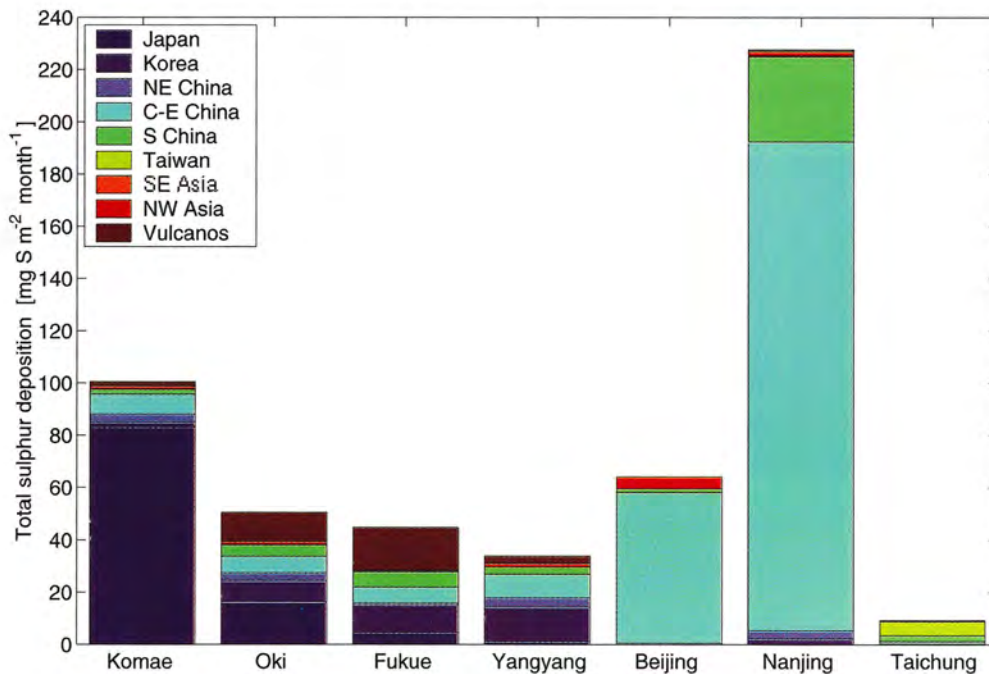


**Figure 29.** As Fig. 28 but for May, 1993.

**Table 10.** Fraction (in %) of total sulphur deposition at 7 East Asian stations emanating from each of the 8 source-regions in Fig. 27 and from volcanic sulphur sources for January 1993, using Task A parameters and extracting total deposition by taking the value in the gridbox containing the station.

|           | Komae | Oki  | Fukue | Yangyang | Beijing | Nanjing | Taichung |
|-----------|-------|------|-------|----------|---------|---------|----------|
| Japan     | 71.6  | 7.5  | 1.4   | 0.0      | 0.0     | 0.0     | 0.0      |
| Korea     | 2.5   | 16.4 | 37.1  | 19.0     | 0.0     | 0.0     | 0.3      |
| NE China  | 4.6   | 36.0 | 5.4   | 51.4     | 0.8     | 1.0     | 1.8      |
| C-E China | 5.5   | 15.7 | 25.7  | 21.1     | 62.5    | 90.5    | 51.5     |
| S China   | 6.8   | 13.8 | 23.0  | 0.9      | 0.0     | 6.7     | 16.7     |
| Taiwan    | 0.2   | 0.0  | 0.3   | 0.0      | 0.0     | 0.0     | 27.6     |
| SE Asia   | 0.6   | 0.7  | 1.9   | 0.0      | 0.0     | 0.5     | 0.3      |
| NW Asia   | 1.6   | 6.9  | 3.5   | 7.5      | 36.6    | 1.2     | 1.9      |
| Volcanic  | 6.5   | 2.9  | 1.6   | 0.0      | 0.0     | 0.0     | 0.0      |

**Table 11.** As Table 10, but for May, 1993.

|           | Komae | Oki  | Fukue | Yangyang | Beijing | Nanjing | Taichung |
|-----------|-------|------|-------|----------|---------|---------|----------|
| Japan     | 82.7  | 32.2 | 10.3  | 3.6      | 0.0     | 0.0     | 0.2      |
| Korea     | 1.8   | 15.9 | 23.6  | 38.6     | 0.0     | 1.0     | 1.6      |
| NE China  | 3.2   | 6.1  | 1.4   | 10.5     | 0.8     | 1.4     | 1.4      |
| C-E China | 7.6   | 12.5 | 13.7  | 26.7     | 89.9    | 82.1    | 10.0     |
| S China   | 1.7   | 8.7  | 12.9  | 8.3      | 2.2     | 14.3    | 24.4     |
| Taiwan    | 0.2   | 0.3  | 0.5   | 0.0      | 0.0     | 0.0     | 58.2     |
| SE Asia   | 0.0   | 0.0  | 0.1   | 0.1      | 0.0     | 0.2     | 0.1      |
| NW Asia   | 1.1   | 2.2  | 1.0   | 3.8      | 7.1     | 0.7     | 3.7      |
| Volcanic  | 1.7   | 22.1 | 36.6  | 8.5      | 0.0     | 0.3     | 0.4      |

## 6. Discussion

Uncertainties in our results stem both from the emission inventory, the chosen parameterisation and the numerical values of the respective parameters, and weaknesses in the driving meteorology. When comparing model results with measurements, an additional source of uncertainty is the question of data representativeness. This is an issue both for the modeller, when he has to choose between different interpolation methods, and for the data collector when he has to assure that his station is representative for a larger region (a model gridbox!). We have shown that natural day-to-day variations at a site are much larger than the differences between simulations with completely different chemical and scavenging parameters. We have also shown that the difference between a “nearest gridpoint” extraction and a “bilinear” extraction of data at a station is comparable to the difference between the simulations with different model parameters. From this we conclude that, within reasonable limits, the driving meteorological data is at least as important as the model formulation. The source-receptor calculations showed large differences between two months. This, again, points towards the importance of the driving meteorology.

## Acknowledgements

Greg Carmichael, Giuseppe Calori, Hiroshi Hayami and all the others at the IIASA meetings for initiating and carrying through the model intercomparison study. Erik Kjellström, Joakim Langner, and Lennart Robertson for comments on earlier versions of this manuscript. Swedish International Development Cooperation Agency (Sida) for financial support administered through Stockholm Environmental Institute (SEI).

## References

- Aardenne van, J.A., Carmichael, G.R., Levy II, H., Streets, D. and Hordijk, L. 1999. Anthropogenic NO<sub>x</sub> emissions in Asia in the period 1990-2020. *Atmos. Environ.* **33**, 633-646.
- Arndt, R.L., Carmichael, G.R. and Roorda, J.M. 1998. Seasonal source-receptor relationships in Asia. *Atmos. Environ.* **32**, 1397-1406.
- Ayers, G., Gillett, R. and Hara, H. 1996. Acidic deposition in East Asia and Oceania. In: *Global acid deposition assessment*. (Eds. D.M. Whelpdale and M.S. Kaiser). **WMO-GAW No. 106; WMO-TD No. 777**. pp. 107-134.
- Carmichael, G.R., Calori, G. Hayami, H. and Uno, I. Model intercomparison study of long range transport and sulfur deposition in East Asia (MICS-ASIA). In: *A comprehensive assessment of large-scale environmental problems in East Asia, Proceeding of the workshop on the transport of air pollutants in Asia 22-23 July 1999*. International Institute for Applied Systems Analysis, Laxenburg, Austria.
- Carmichael, G.R., Ferm, M., Adikary, S., Ahmad, J., Mohan, M., Hong, M.-S., Chen, L., Fook, L., Liu, C.M., Soedomo, M., Tran, G., Suksosank, K., Zhao, D., Arndt, R. and Chen, L.L. 1995. Observed regional distribution of sulfur dioxide in Asia. *Water, Air, and Soil Pollution* **85**, 2289-2294.
- Engardt, M. and Holmén, K. 1996. Towards deducing regional sources and sinks from atmospheric CO<sub>2</sub> measurements at Spitsbergen. *Physics and Chemistry of the Earth* **21**, 523-528.
- Engardt, M. and Holmén, K. 1999. Model simulations of anthropogenic-CO<sub>2</sub> transport to an Arctic monitoring station during winter. *Tellus* **51B**, 194-209.
- Ferm, M. and Rodhe, H. 1997. Measurements of air concentrations of SO<sub>2</sub>, NO<sub>2</sub> and NH<sub>3</sub> at rural and remote sites in Asia. *Atmos. Environ.* **27**, 17-29.
- Granat, L., Suksomsankh, K., Simachaya, S., Tabucanon, M. and Rodhe, H. 1996. Regional background acidity and chemical composition of precipitation in Thailand. *Atmos. Environ.* **30**, 1589-1596.
- Hayami, H., Fujita, S., Ichikawa, Y., Huang, T.C., Lee, C.K., Jeng, F.T., Chang, J.S., Chang, K.H. and Lin P.L. 1999. *Joint report on regional acid deposition in East Asia*. **CRIEPI Report T989802**.
- Hayami, H. and Ichikawa, Y. 1995. Development of hybrid LRT model to estimate sulfur deposition in Japan. *Water Air and Soil Pollution* **85**, 2015-2020.
- Hicks, K., Kuylenstierna, J., Robertson, L. and Granat, L. 1998. Atmospheric transfer and deposition. In: *Regional air pollution in developing countries. Background document for policy dialogue, Bangkok, March 1998*. (Eds. J. Kuylenstierna and K. Hicks). Stockholm Environment Institute, pp. 73-86.
- Ichikawa, Y. and Fujita, S. 1995. An analysis of wet deposition of sulfate using a trajectory model for East Asia. *Water Air and Soil Pollution* **85**, 1927-1932.
- Kuylenstierna, J.C.I., Cambridge, H., Cinderby, S. and Chadwick, M.J. 1995. Terrestrial ecosystem sensitivity to acidic deposition in developing countries. *Water, Air, and Soil Pollution* **85**, 2319-2324.
- Langner, J., Persson, C. and Robertson, L. 1995. Concentration and deposition of acidifying air pollutants over Sweden: Estimates 1991 based on the MATCH model and observations. *Water Air and Soil Pollution* **85**, 2021-2026.
- Langner, J., Persson, C., Robertson, L. and Ullerstig, A. 1996. *Air pollution Assessment Study Using the MATCH Modelling System. Application to sulfur and nitrogen compounds over Sweden 1994*. Swedish Meteorological and Hydrological Institute, **Report RMK No. 69**. ?? pp.

- Langner, J., Bergström, R. and Pleijel, K. 1998a. *European scale modeling of sulfur, oxidised nitrogen and photochemical oxidants. Model evaluation for the 1994 growing season.* Swedish Meteorological and Hydrological Institute, **Report RMK No. 82**, 71 pp.
- Langner, J., Robertson, L., Persson, C. and Ullerstig, A. 1998b. Validation of the operational emergency response model at the Swedish meteorological and hydrological institute using data from ETEX and the Chernobyl accident. *Atmos. Environ.* **32**, 4325-4333.
- Lefohn, A.S., Husar, J.D. and Husar, R.B. 1999. Estimating historical anthropogenic global sulfur emission patterns for the period 1850-1990. *Atmos. Environ.* **33**, 3435-3444.
- Louis, J.-F. 1979. A parametric model of the vertical eddy fluxes in the atmosphere. *Boundary-Layer Meteor.* **17**, 187-201.
- Phadnis, M.J., Carmichael, G.R., Ichikawa, Y. and Hayami, H. 1998. Evaluation of long range transport models for acidic deposition in East Asia. *J. Appl. Meteor.* **37**, 1127-1142.
- Robertson, L., Rodhe H. and Granat, L. 1995. Modelling of sulfur deposition in the southern Asian region. *Water, Air and Soil Pollution* **85**, 2337-2343.
- Robertson, L. 1996. *Modelling of anthropogenic sulfur deposition to the African and South American continents.* Swedish Meteorological and Hydrological Institute, **Report RMK No. 73**, 10 pp.
- Robertson, L., Langner, J. and Engardt, M. 1996. *MATCH - Meso-scale Atmospheric Transport and Chemistry modelling system. Basic transport model description and control experiments with <sup>222</sup>Rn.* Swedish Meteorological and Hydrological Institute, **Report RMK No. 70**, 37 pp.
- Robertson, L. and Langner, J. 1998. Source function estimate by means of variational data assimilation applied to the ETEX-1 tracer experiment. *Atmos. Environ.* **32**, 4219-4225.
- Robertson, L., Langner, J. and Engardt, M. 1999. An Eulerian limited-area atmospheric transport model. *J. Appl. Meteor.* **38**, 190-210.
- Rodhe, H. 1999. Human impact on the atmospheric sulfur balance. *Tellus* **51AB**, 110-122.
- Rodhe, H., Galloway, J. and Dianwu, Z. 1992. Acidification in Southeast Asia – Prospects for the coming decades. *Ambio* **21**, 148-150.
- Rodhe, H., Grennfelt, P., Wisniewski, J., Ågren, C., Bengtsson, G., Johansson, K., Kauppi, P., Kucera, V., Rasmussen, L., Rosseland, B., Schotte, L. and Selldén, G. 1995. Acid Reign '95? - Conference summary statement. *Water, Air and Soil Pollution* **85**, 1-14.
- Streets, D.G., Carmichael, G.R., Amann, M. and Arndt, R.L. 1999. Energy consumption and acid deposition in Northeast Asia. *Ambio* **28**, 135-143.
- Streets, D.G. and Waldhoff, S.T. 1999. Present and future emissions of air pollutants in China: SO<sub>2</sub>, NO<sub>x</sub>, and CO. *Atmos. Environ.* **34**, 363-374.
- Tarrasón, L. and Iversen, T. 1998. Modelling intercontinental transport of atmospheric sulphur in the northern hemisphere. *Tellus* **50B**, 331-352.
- Xu, Y. and Carmichael, G.R. 1998. Modeling the dry deposition velocity of sulfur dioxide and sulfate in Asia. *J. Appl. Meteor.* **37**, 1084-1099.
- Xu, Y. and Carmichael, G.R. 1999. An assessment of sulfur deposition pathways in Asia. *Atmos. Environ.* **33**, 3473-3486.



## SMHI's publications

SMHI publishes six report series. Three of these, the R-series, are intended for international readers and are in most cases written in English. For the others the Swedish language is used.

### Names of the Series

### Published since

|  |      |
|--|------|
| RMK (Report Meteorology and Climatology) | 1974 |
| RH (Report Hydrology)                    | 1990 |
| RO (Report Oceanography)                 | 1986 |
| METEOROLOGI                              | 1985 |
| HYDROLOGI                                | 1985 |
| OCEANOGRAFI                              | 1985 |

### Earlier issues published in serie RMK

- |   |   |    |   |
|---|---|----|---|
| 1 | Thompson, T., Udin, I., and Omstedt, A. (1974)<br>Sea surface temperatures in waters surrounding Sweden.                              | 8  | Eriksson, B. (1977)<br>Den dagliga och årliga variationen av temperatur, fuktighet och vindhastighet vid några orter i Sverige. |
| 2 | Bodin, S. (1974)<br>Development on an unsteady atmospheric boundary layer model.  | 9  | Holmström, I., and Stokes, J. (1978)<br>Statistical forecasting of sea level changes in the Baltic.                             |
| 3 | Moen, L. (1975)<br>A multi-level quasi-geostrophic model for short range weather predictions.   | 10 | Omstedt, A., and Sahlberg, J. (1978)<br>Some results from a joint Swedish-Finnish sea ice experiment, March, 1977.              |
| 4 | Holmström, I. (1976)<br>Optimization of atmospheric models.   | 11 | Haag, T. (1978)<br>Byggnadsindustrins väderberoende, seminarieuppsats i företagsekonomi, B-nivå.                                |
| 5 | Collins, W.G. (1976)<br>A parameterization model for calculation of vertical fluxes of momentum due to terrain induced gravity waves. | 12 | Eriksson, B. (1978)<br>Vegetationsperioden i Sverige beräknad från temperaturobservationer.                                     |
| 6 | Nyberg, A. (1976)<br>On transport of sulphur over the North Atlantic.   | 13 | Bodin, S. (1979)<br>En numerisk prognosmodell för det atmosfäriska gränsskiktet, grundad på den turbulenta energiekvationen.    |
| 7 | Lundqvist, J.-E., and Udin, I. (1977)<br>Ice accretion on ships with special emphasis on Baltic conditions.                           | 14 | Eriksson, B. (1979)<br>Temperaturfluktuationer under senaste 100 åren.  |

- 15 Udin, I., och Mattisson, I. (1979)  
Havsis- och snöinformation ur datorbearbetade satellitdata - en modellstudie.
- 16 Eriksson, B. (1979)  
Statistisk analys av nederbördsdata. Del I. Arealnederbörd.
- 17 Eriksson, B. (1980)  
Statistisk analys av nederbördsdata. Del II. Frekvensanalys av månadsnederbörd.
- 18 Eriksson, B. (1980)  
Årsmedelvärden (1931-60) av nederbörd, avdunstning och avrinning.
- 19 Omstedt, A. (1980)  
A sensitivity analysis of steady, free floating ice.
- 20 Persson, C., och Omstedt, G. (1980)  
En modell för beräkning av luftföreningars spridning och deposition på mesoskala.
- 21 Jansson, D. (1980)  
Studier av temperaturinversioner och vertikal vindskjuvning vid Sundsvall-Härnösands flygplats.
- 22 Sahlberg, J., and Törnevik, H. (1980)  
A study of large scale cooling in the Bay of Bothnia.
- 23 Ericson, K., and Hårsmar, P.-O. (1980)  
Boundary layer measurements at Klock-rike. Oct. 1977.
- 24 Bringfelt, B. (1980)  
A comparison of forest evapotranspiration determined by some independent methods.
- 25 Bodin, S., and Fredriksson, U. (1980)  
Uncertainty in wind forecasting for wind power networks.
- 26 Eriksson, B. (1980)  
Graddagsstatistik för Sverige.
- 27 Eriksson, B. (1981)  
Statistisk analys av nederbördsdata. Del III. 200-åriga nederbördsserier.
- 28 Eriksson, B. (1981)  
Den "potentiella" evapotranspirationen i Sverige.
- 29 Pershagen, H. (1981)  
Maximisnödjunp i Sverige (perioden 1905-70).
- 30 Lönnqvist, O. (1981)  
Nederbördsstatistik med praktiska tillämpningar. (Precipitation statistics with practical applications.)
- 31 Melgarejo, J.W. (1981)  
Similarity theory and resistance laws for the atmospheric boundary layer.
- 32 Liljas, E. (1981)  
Analys av moln och nederbörd genom automatisk klassning av AVHRR-data.
- 33 Ericson, K. (1982)  
Atmospheric boundary layer field experiment in Sweden 1980, GOTEX II, part I.
- 34 Schoeffler, P. (1982)  
Dissipation, dispersion and stability of numerical schemes for advection and diffusion.
- 35 Undén, P. (1982)  
The Swedish Limited Area Model. Part A. Formulation.
- 36 Bringfelt, B. (1982)  
A forest evapotranspiration model using synoptic data.
- 37 Omstedt, G. (1982)  
Spridning av luftförorening från skorsten i konvektiva gränsskikt.
- 38 Törnevik, H. (1982)  
An aerobiological model for operational forecasts of pollen concentration in the air.
- 39 Eriksson, B. (1982)  
Data rörande Sveriges temperaturklimat.
- 40 Omstedt, G. (1984)  
An operational air pollution model using routine meteorological data.
- 41 Persson, C., and Funkquist, L. (1984)  
Local scale plume model for nitrogen oxides. Model description.

- 42 Gollvik, S. (1984)  
Estimation of orographic precipitation by dynamical interpretation of synoptic model data.
- 43 Lönnqvist, O. (1984)  
Congression - A fast regression technique with a great number of functions of all predictors.
- 44 Laurin, S. (1984)  
Population exposure to SO and NO<sub>x</sub> from different sources in Stockholm.
- 45 Svensson, J. (1985)  
Remote sensing of atmospheric temperature profiles by TIROS Operational Vertical Sounder.
- 46 Eriksson, B. (1986)  
Nederbörds- och humiditetsklimat i Sverige under vegetationsperioden.
- 47 Taesler, R. (1986)  
Köldperioden av olika längd och förekomst.
- 48 Wu Zengmao (1986)  
Numerical study of lake-land breeze over Lake Vättern, Sweden.
- 49 Wu Zengmao (1986)  
Numerical analysis of initialization procedure in a two-dimensional lake breeze model.
- 50 Persson, C. (1986)  
Local scale plume model for nitrogen oxides. Verification.
- 51 Melgarejo, J.W. (1986)  
An analytical model of the boundary layer above sloping terrain with an application to observations in Antarctica.
- 52 Bringfelt, B. (1986)  
Test of a forest evapotranspiration model.
- 53 Josefsson, W. (1986)  
Solar ultraviolet radiation in Sweden.
- 54 Dahlström, B. (1986)  
Determination of areal precipitation for the Baltic Sea.
- 55 Persson, C. (SMHI), Rodhe, H. (MISU), De Geer, L.-E. (FOA) (1986)  
The Chernobyl accident - A meteorological analysis of how radionucleides reached Sweden.
- 56 Persson, C., Robertson, L. (SMHI), Grennfelt, P., Kindbom, K., Lövblad, G., och Svanberg, P.-A. (IVL) (1987)  
Luftföroreningsepisoden över södra Sverige 2 - 4 februari 1987.
- 57 Omstedt, G. (1988)  
An operational air pollution model.
- 58 Alexandersson, H., Eriksson, B. (1989)  
Climate fluctuations in Sweden 1860 - 1987.
- 59 Eriksson, B. (1989)  
Snödjupsförhållanden i Sverige - Säsongerna 1950/51 - 1979/80.
- 60 Omstedt, G., Szegö, J. (1990)  
Människors exponering för luftföroreningar.
- 61 Mueller, L., Robertson, L., Andersson, E., Gustafsson, N. (1990)  
Meso- $\gamma$  scale objective analysis of near surface temperature, humidity and wind, and its application in air pollution modelling.
- 62 Andersson, T., Mattisson, I. (1991)  
A field test of thermometer screens.
- 63 Alexandersson, H., Gollvik, S., Mueller, L. (1991)  
An energy balance model for prediction of surface temperatures.
- 64 Alexandersson, H., Dahlström, B. (1992)  
Future climate in the Nordic region - survey and synthesis for the next century.
- 65 Persson, C., Langner, J., Robertson, L. (1994)  
Regional spridningsmodell för Göteborgs och Bohus, Hallands och Älvsborgs län. (A mesoscale air pollution dispersion model for the Swedish west-coast region. In Swedish with captions also in English.)
- 66 Karlsson, K.-G. (1994)  
Satellite-estimated cloudiness from NOAA AVHRR data in the Nordic area during 1993.

- 67 Karlsson, K-G. (1996)  
Cloud classifications with the SCANDIA model.
- 68 Persson, C., Ullerstig, A. (1996)  
Model calculations of dispersion of lindane over Europe. Pilot study with comparisons to measurements around the Baltic Sea and the Kattegat.
- 69 Langner, J., Persson, C., Robertson, L., and Ullerstig, A. (1996)  
Air pollution Assessment Study Using the MATCH Modelling System. Application to sulfur and nitrogen compounds over Sweden 1994.
- 70 Robertson, L., Langner, J., Engardt, M. (1996)  
MATCH - Meso-scale Atmospheric Transport and Chemistry modelling system.
- 71 Josefsson, W. (1996)  
Five years of solar UV-radiation monitoring in Sweden.
- 72 Persson, C., Ullerstig, A., Robertson, L., Kindbom, K., Sjöberg, K. (1996)  
The Swedish Precipitation Chemistry Network. Studies in network design using the MATCH modelling system and statistical methods.
- 73 Robertson, L. (1996)  
Modelling of anthropogenic sulfur deposition to the African and South American continents.
- 74 Josefsson, W. (1996)  
Solar UV-radiation monitoring 1996.
- 75 Häggmark, L., Ivarsson, K.-I. (SMHI), Olofsson, P.-O. (Militära vädertjänsten). (1997)  
MESAN - Mesoskalig analys.
- 76 Bringfelt, B, Backström, H, Kindell, S, Omstedt, G, Persson, C, Ullerstig, A. (1997)  
Calculations of PM-10 concentrations in Swedish cities- Modelling of inhalable particles
- 77 Gollvik, S. (1997)  
The Teleflood project, estimation of precipitation over drainage basins.
- 78 Persson, C., Ullerstig, A. (1997)  
Regional luftmiljöanalys för Västmanlands län baserad på MATCH modell-beräkningar och mätdata - Analys av 1994 års data
- 79 Josefsson, W., Karlsson, J.-E. (1997)  
Measurements of total ozone 1994-1996.
- 80 Rummukainen, M. (1997)  
Methods for statistical downscaling of GCM simulations.
- 81 Persson, T. (1997)  
Solar irradiance modelling using satellite retrieved cloudiness - A pilot study
- 82 Langner, J., Bergström, R. (SMHI) and Pleijel, K. (IVL) (1998)  
European scale modelling of sulfur, oxidized nitrogen and photochemical oxidants. Model development and evaluation for the 1994 growing season.
- 83 Rummukainen, M., Räisänen, J., Ullerstig, A., Bringfelt, B., Hansson, U., Graham, P., Willén, U. (1998)  
RCA - Rossby Centre regional Atmospheric climate model: model description and results from the first multi-year simulation.
- 84 Räisänen, J., Döschner, R. (1998)  
Simulation of present-day climate in Northern Europe in the HadCM2 OAGCM.
- 85 Räisänen, J., Rummukainen, M., Ullerstig, A., Bringfelt, B., Ulf Hansson, U., Willén, U. (1999)  
The First Rossby Centre Regional Climate Scenario - Dynamical Downscaling of CO<sub>2</sub>-induced Climate Change in the HadCM2 GCM.
- 86 Rummukainen, Markku. (1999)  
On the Climate Change debate
- 87 Räisänen, Jouni (2000)  
CO<sub>2</sub>-induced climate change in northern Europe: comparison of 12 CMIP2 experiments.









Swedish Meteorological and Hydrological Institute  
SE 601 76 Norrköping, Sweden.  
Tel +46 11-495 80 00. Fax +46 11-495 80 01